Biotechnology Advances 34 (2016) 250–271

Contents lists available at ScienceDirect

Biotechnology Advances

journal homepage: www.elsevier.com/locate/biotechadv

Photonic hydrogel sensors☆

Ali K. Yetisen [a,**], Haider Butt [b], Lisa R. Volpatti [c], Ida Pavlichenko [d], Matjaž Humar [a,e], Sheldon J.J. Kwok [a,f], Heebeom Koo [a], Ki Su Kim [a], Izabela Naydenova [g], Ali Khademhosseini [f,h,i,j,l], Sei Kwang Hahn [k], Seok Hyun Yun [a,f,*]

[a] Harvard Medical School, Wellman Center for Photomedicine, Massachusetts General Hospital, 65 Landsdowne Street, Cambridge, MA 02139, USA
[b] School of Mechanical Engineering, University of Birmingham, Edgbaston, Birmingham B15 2TT, United Kingdom
[c] Department of Chemical Engineering, Massachusetts Institute of Technology, 77 Massachusetts Avenue, Cambridge, MA 02139, USA
[d] School of Engineering and Applied Sciences, Harvard University, 9 Oxford Street, Cambridge, MA 02139, USA
[e] Condensed Matter Department, J. Stefan Institute, Jamova 39, SI-1000 Ljubljana, Slovenia
[f] Harvard-MIT Division of Health Sciences and Technology, Massachusetts Institute of Technology, Cambridge, MA 02139, USA
[g] Centre for Industrial and Engineering Optics, School of Physics, College of Sciences and Health, Dublin Institute of Technology, Dublin 8, Ireland
[h] Biomaterials Innovation Research Center, Division of Biomedical Engineering, Brigham and Women's Hospital, Harvard Medical School, Cambridge, MA 02139, USA
[i] Wyss Institute for Biologically Inspired Engineering, Harvard University, Boston, MA 02115, USA
[j] Department of Physics, King Abdulaziz University, Jeddah, Saudi Arabia
[k] Department of Materials Science & Engineering, Pohang University of Science and Technology (POSTECH), 77 Cheongam-ro, Nam-gu, Pohang, Kyungbuk 790-784, Republic of Korea
[l] Department of Bioindustrial Technologies, College of Animal Bioscience and Technology, Konkuk University, Hwayang-dong, Gwangjin-gu, Seoul 143-701, Republic of Korea

ARTICLE INFO

Article history:
Received 20 June 2015
Received in revised form 11 October 2015
Accepted 16 October 2015
Available online 17 October 2015

Keywords:
Hydrogels
In vitro diagnostics
Photonic crystals
Inverse opals
Holography
Bragg stacks
Crystalline colloidal arrays
Block copolymers
Layer-by-layer deposition
Plasmonics

ABSTRACT

Analyte-sensitive hydrogels that incorporate optical structures have emerged as sensing platforms for point-of-care diagnostics. The optical properties of the hydrogel sensors can be rationally designed and fabricated through self-assembly, microfabrication or laser writing. The advantages of photonic hydrogel sensors over conventional assay formats include label-free, quantitative, reusable, and continuous measurement capability that can be integrated with equipment-free text or image display. This Review explains the operation principles of photonic hydrogel sensors, presents syntheses of stimuli-responsive polymers, and provides an overview of qualitative and quantitative readout technologies. Applications in clinical samples are discussed, and potential future directions are identified.

1. Introduction

1.1. The need for photonic sensors

The *in vitro* diagnostics (IVD) market was valued at $53.3 B in 2013 and projected to reach $69.1 B by 2017 (Markets&Markets, 2013; Shields and Sale, 2014). While the global IVD market is expected to grow at a compound annual growth rate (CAGR) of 5.4% until 2020, the emerging markets (Brazil, China, and India) are projected to experience 10–15% growth (Grand View Research, 2014; Park, 2014; Rosen, 2014). This growth is mainly driven by (i) the shift to personalized medicine, (ii) the need for minimally invasive rapid diagnostics, (iii) aging populations in the developed world, and (iv) geographical market expansion and the increase in the demand from emerging economies due to infectious and chronic diseases (Akram et al., 2015; Yetisen et al., 2015b). Although the market is restrained by stringent regulations (Mansfield et al., 2005), there is a growing number of commercial products such as diagnostic tests for HIV, hepatitis, HPV, diabetes, blood coagulation, fertility, immunoassays, hematology, urinalysis, molecular diagnostics, and blood gas analyses (Roche, 2014; Siemens, 2014).

The fastest growing segments of the IVD market are molecular diagnostics and point-of-care (POC) testing, which have attracted

☆ Biotechnology Advances Special Issue: Trends in IVD and Mobile Healthcare.

* Corresponding author.
** Correspondence to: A.K. Yetisen, Harvard Medical School, Wellman Center for Photomedicine, Massachusetts General Hospital, 65 Landsdowne Street, Cambridge, MA 02139, USA.
E-mail addresses: ayetisen@mgh.harvard.edu (A.K. Yetisen), syun@mgh.harvard.edu (S.H. Yun).

http://dx.doi.org/10.1016/j.biotechadv.2015.10.005
0734-9750/

$650 million in investments over the past five years (Kalorama Information, 2014; Parmar, 2013; St John and Price, 2014). The expansion of POC diagnostics may be attributed to the government policies to reduce high-cost healthcare provisions by decreasing the number of patients in secondary and tertiary hospitals (Price and Kricka, 2007). POC diagnostics consist of small benchtop or handheld devices that provide qualitative and semi-quantitative information of target analytes in the field or at home (Chin et al., 2012). Benchtop products include critical care analyzers, as well as hematology and immunology assays. Handheld devices consist of blood glucose tests, dipsticks for urinalysis and lateral-flow tests (Yetisen et al., 2013). These handheld devices are simple, rapid, robust in storage and usage, and low cost. Thus, they are universally applicable for disposable and sensitive POC diagnostics. The sensing mechanisms of handheld POC diagnostics are based on molecular probes, enzymes, antibody–antigen interactions, and electrochemistry. Dipstick tests such as urine test strips utilize molecular dyes and enzymatic reactions. Such assays are multiplexed and allow the analyses of up to 12 biomarkers. Recently, new capabilities have been proposed for these formats to execute multistep processes (Cate et al., 2015). A significant limitation of assays based on molecular dyes is that they have different absorption peaks in the visible spectrum (Martinez et al., 2008). The interpretation of such assays may be erroneous due to the subjective readouts and uneven development of colors throughout the surface. Their semi-quantitative readouts require handheld analyzers. Additionally, the number of analytes and molecular reactions that can be combined with chromogens is limited. Hence, standardization of color shift in the visible spectrum and expansion to a broad range of analytes are significant challenges in molecular dye based assays (Yetisen, 2015f). Furthermore, while the colorimetric information is universal, some applications require written readouts for reporting the concentration of a target analyte. The lateral-flow format is typically based on immunochromatography involving immobilized antibodies and functionalized gold nanoparticles, which were originally designed for qualitative readouts. Recently, newer capabilities were introduced to this platform to obtain semi-quantitative readouts. For example, ClearblueDigital Pregnancy Test (Swiss Precision Diagnostics) offers on-chip quantification of chorionic gonadotropin (hCG) to estimate the conception date (Pike et al., 2013). Among the over the counter products, blood glucose monitoring is the largest market segment due to the prevalence of 382 million diagnosed diabetics worldwide (Danaei et al., 2011; Diabetes Atlas, 2013). Glucose assays are based on enzymes such as glucose oxidase (GOx), glucose dehydrogenase (GDH) or hexokinase, which are read out by handheld devices. However, such electrochemical and enzymatic assays are prone to error due to interference from high partial pressure of oxygen, maltose, and hematocrit (Tonyushkina and Nichols, 2009). Additionally, these assays do not allow real-time or on-demand reusable measurements due to the irreversibility of reactions and assay configurations. The development of all-in-one platforms that can report on the concentrations of target analytes by either utilizing the entire visible spectrum, or producing written information or display images without electrical components is needed to create low-cost, robust and quantitative POC diagnostics.

The limitations of the existing sensors have motivated the investigation of label-free structural color platforms that quantitatively report on the concentration of target analytes (Zhao et al., 2010a). Structural coloration was first observed by Robert Hooke and Isaac Newton in peacock feathers and mother of pearl (nacre) (Hooke, 1665; Newton, 1704). To understand structural coloration, Thomas Young demonstrated that light could behave like a wave, producing diffraction from sharp edges or slits (Young, 1804). A wide array of mechanisms has evolved to create diverse optical structures, including multilayer reflectors, photonic crystals, and light scattering structures (Fudouzi, 2011; Zhao et al., 2012). These structural colors also coincidentally form in composite and fibrous structures (Martinez-Hurtado et al., 2013; Vignolini et al., 2012; Vukusic and Sambles, 2003). Structural coloration in nature occurs mainly through diffraction, but also refraction, plasmonics, or a combination of both, sometimes complementing pigments. The fundamentals of dynamic coloration in photonic structures in nature represent a potential for constructing transducers that can be modulated by physical changes.

Structural color-based transducers have advantages over traditional signal processing approaches in terms of response-range tuning and label-free reporting. Advances in photography, polymer chemistry, laser physics, and organic synthesis have enabled bottom-up and top-down fabrication of photonic structural colors. Hence, the developments in photonic structures have set the stage for the incorporation of structural colors in analyte-sensitive hydrophilic polymers (hydrogels) for sensing applications. In contrast to the absorption of light by chromophores and electrochemistry, photonic hydrogel sensors incorporate nanostructures that modulate the optical properties of incident light. Such photonic structures can be created in/on hydrogels through self-assembly or laser writing techniques. Upon interacting with a target analyte, hydrogels undergo volumetric changes, which affect the physical and/or optical properties of the photonic structures. These photonic structures serve as transducers to quantify the concentration of analytes through changes in spatial periodicity in their dielectric constants, plasmonic resonance shifts, or effective refractive index. They typically modulate the optical characteristics of electromagnetic waves by filtering out certain regions of wavelengths, a phenomenon called the photonic band gap (PBG), which typically occurs in 1D Bragg gratings as well as 2D and 3D (dimensional) colloidal photonic crystals (Joannopoulos et al., 2011). However, the filtering mechanism of these sensors may include Fabry–Pérot interferometer (etalon), or thin film effects.

This Review presents the operation principles of photonic hydrogel sensors. It describes the syntheses of analyte-sensitive hydrogel matrixes and explains bottom-up and top-down nano/microfabrication methods to incorporate structures within hydrogels that act as optical transducers. The technical challenges in sensor fabrication are identified, and pre-clinical and clinical performance evaluations are presented. This Review also discusses how photonic hydrogel sensors can address IVD market needs. The perceived limitations of photonic hydrogel sensors in building commercial products are identified, and potential future directions are described.

1.2. Historical development of diffraction gratings in hydrogels

Experimentation with gels in optics began in the 19th century. Frederick Archer invented the collodion process, which utilized albumen (egg white) photographic prints (Archer, 1851; Blanquart-Evrard, 1847). To improve the collodion process, Richard Maddox reported a method to create photographic images in gelatin (Maddox, 1871). Two decades later, Gabriel Lippmann introduced a technique to create color photographs based on interference of light (Lippmann, 1894). Lippmann projected an image onto a silver bromide containing photographic emulsion, which was backed by a mirror of liquid mercury. The light reflected back by the mirror created standing waves in the emulsion. This latent image was later photographically developed to produce periodic silver planes. When illuminated with a broadband light source, the plate replayed a colored image *via* diffraction. After the development of the principle of holography in the 1940s (Gabor, 1948, 1949) and invention of laser in the 1950s (Maiman, 1960), Yuri Denisyuk of the former Soviet Union, and Emmett Leith and Juris Upatnieks in the United States created 3D holographic gratings in gelatin (Denisyuk, 1962; Leith and Upatnieks, 1962). In parallel to the developments in holography, hydrogel chemistry also made significant advances (Loh and Scherman, 2012). Poly(*N*-isopropylacrylamide) (PNIPAAm) was first synthesized in Rohm & Haas Company (Philadelphia, PA) (Specht et al., 1956); however, its thermal expansion properties in aqueous solutions were realized after a decade (Heskins and Guillet, 1968). In the former Czechoslovakia, Otto Wichterle and

Drahoslav Lím developed poly(2-hydroxyethyl methacrylate) (pHEMA) for application in soft contact lenses (Wichterle and Lim, 1960).

The advantages of incorporating diffraction gratings in polymers matrixes have been realized by Thomson-CSF (France) (Loiseaux et al., 1984). This approach involved forming a medium consisting of suspended dielectric nanoparticles (~20 nm) in a monomer solution. Standing waves consisting of high (antinodes) and low (nodes, no disturbance) energy induced by holographic optical forces moved the nanoparticles into periodic regions. Subsequently, nanoparticles were fixed to their positions by polymerizing the monomer solution. It was not until 1990s that the use of holographic gratings in biosensing applications was proposed by Christopher R. Lowe at the University of Cambridge (Lowe et al., 1995). Holograms were used as recording media to create diffraction gratings in functionalized hydrogel matrixes and the principle of operation of hydrogel-based optical sensors was demonstrated. Independently, Sanford Asher at the University of Pittsburgh have developed crystalline colloidal arrays (CCAs) for narrow-band filtering devices in the visible spectrum and UV (Asher, 1986). In their earlier work, the liquid dispersion was contained in a thin planar cell within walls of transparent plastics or glass. However, a significant challenge with the utilization of the CCAs was their fragility, and the arrays were affected from vibration, temperature changes, and ionic influences. Hence, in the 1990s, CCAs were incorporated in hydrogel films (Haacke et al., 1993). Based on CCAs, Asher and co-workers developed hydrogel sensors (Asher and Holtz, 1998). Along with the advances in recognition agents, photonic hydrogel sensors opened up applications for IVD.

1.3. The prospects for photonic hydrogel sensors

Photonic structures embedded in hydrogels that change their water content and volume upon interacting with a specific analyte represent a new platform to construct IVD devices. Hydrogels are 3D polymer networks capable of undergoing reversible volume changes as their Donnan osmotic pressure varies (Imran et al., 2010; Miyata, 2010). Hydrogels can be synthesized to be sensitive to a range of clinically relevant analytes (Stuart et al., 2010; Um et al., 2006; Kloxin et al., 2009; Lendlein et al., 2005; Ehrick et al., 2005; Ehrbar et al., 2008; Cai et al., 2015; Banwell et al., 2009). These hydrogels consist of bioactive recognition molecules that selectively respond to external stimuli *via* producing physical or chemical changes (Buenger et al., 2012; Loh and Scherman, 2012). Functionalized hydrogels can be used as a medium to incorporate photonic structures for optical signal transduction and reporting within one device. Numerous bottom-up or top-down nano/microfabrication methods have been developed to create photonic structures in miniaturized and multiplexed formats (Zhao et al., 2010a). Upon interacting with a target analyte, the volumetric change in the hydrogel is reported through modulations of reflection, diffraction, refraction, surface plasmon resonance, or emission (Gerlach and Arndt, 2009). These optical changes act as transducers, allowing various light properties to be analyzed spectroscopically and correlated with the concentration of the analyte. Additionally, photonic hydrogel sensors can be tuned to report visually-distinguishable color changes that can be semi-quantitatively determined without equipment. The most important advantage of photonic hydrogel sensors over established assay formats is that they do not rely on labels or electrochemistry to report on the concentration of a target analyte; hence, they are immune to marker bleaching, signal drifts, and electromagnetic interference. Photonic hydrogel sensors (i) incorporate functionalized polymers to respond to a target analyte, (ii) offer reversible real-time measurement of analytes, (iii) can be tuned to report the concentration of analytes colorimetrically from ultraviolet to near-infrared, and (iv) are compatible with readout devices for quantitative measurements. These photonic hydrogels may also have optically active elements with capabilities in displaying 3D images or writing (Naydenova et al., 2008). Hence, the development of photonic hydrogel sensors has immense potential for both equipment-free semi-quantitative diagnostics and quantitative analyzers that are compatible with mobile spectrophotometers and smartphone readers (Burgess et al., 2013; Yetisen, 2015e).

The potential applications of photonic hydrogel sensors are not limited to medical diagnostics, but also include veterinary testing, pharmaceutical bioassays, and biohazard and environmental monitoring. However, the main focus area of hydrogel sensors has been in the detection and/or quantification of chemicals and cells in medical diagnostics. For example, their potential applications in biochemistry and biology are monitoring enzyme activity and metabolites (Tian et al., 2014), and serum albumin ligand binding (Cai et al., 2014). Another potential area of application of photonic hydrogel sensors includes the detection of biocontaminants, heavy metals, and nanoparticles in water or air. The development of environmental sensors is aligned with the strict regulations imposed by the European Union, and the United States. Reusable hydrogel-based sensing of environmental contaminants is an emerging area that can significantly reduce the costs and turnaround time at resource-limited settings.

2. Photonic band-gap hydrogels

Bragg diffraction of light from nanoscale periodic structures can be designed to be dependent on the presence of analytes in a controlled way and therefore can be employed to create sensors reporting from ultraviolet to near-infrared regions. (Ge and Yin, 2011). Periodic structures within hydrogel matrixes can be formed using nanostructures, or can consist of different block copolymers or layers of polyelectrolytes. The specificity of such sensors is achieved by functionalizing the hydrogel matrix with chelating agents or ligands pre- or post-polymerization (Zhao et al., 2010a). Bottom-up and top-down fabrication techniques include laser writing of gratings (Yetisen et al., 2014f), colloidal self-assembly (Cai et al., 2015), pore etching (DeLouise et al., 2005), spincoating (von Freymann et al., 2013), block-co-polymerization (Kim et al., 2010), and layer-by-layer deposition (Kotov, 1999).

2.1. Holographic sensors

Holograms can be used as analytical devices to quantify the humidity content and biomolecule concentration (Blyth et al., 1996; Lowe et al., 1995; Millington et al., 1996; Spooncer et al., 1992). Holographic sensors incorporate multilayer Bragg diffraction gratings in functionalized hydrogel matrixes. Altering the lattice spacing, the effective refractive index, and/or the refractive index modulation of the Bragg grating changes the characteristics of the diffracted or transmitted light (Yetisen, 2015a). For example, in reflection holograms, swelling or shrinking of the polymer matrix shifts the Bragg peak to longer or shorter wavelengths, and the change in the position of the Bragg peak is correlated with the concentration of the analyte that is being measured (Fig. 1a). The diffraction grating in the hologram acts as a reporter allowing changes in the color to be monitored semi-quantitatively by eye, or quantitatively using a spectrophotometer or a smartphone camera. The advantage of holographic sensors over other photonic hydrogel sensors is the ability to accurately fabricate Bragg gratings using laser light.

The design of a holographic sensor involves determining (i) monomers to construct a hydrogel matrix, (ii) a bioactive recognition group, and (iii) an image recording technique (Yetisen, 2015d). Commonly used monomers include HEMA, acrylamide (AAm), vinyl alcohol (VA), and siloxane derivatives. These monomers can be polymerized over a silanized glass or an O_2 plasma-treated plastic substrate in the presence of crosslinkers using photoinitiators such as 2,2-dimethoxy-2-phenylacetophenone (DMPA), or thermal initiators such as *N*,*N*,*N*′,*N*′-tetramethylethylenediamine (TEMED) (Tsangarides et al., 2014). A range of functional groups can be added to the monomer mixture to create specificity for target analytes. These include carboxylic acid (CA), crown ethers, 8-hydroxyquinoline, porphyrin, and phenyl boronic acid

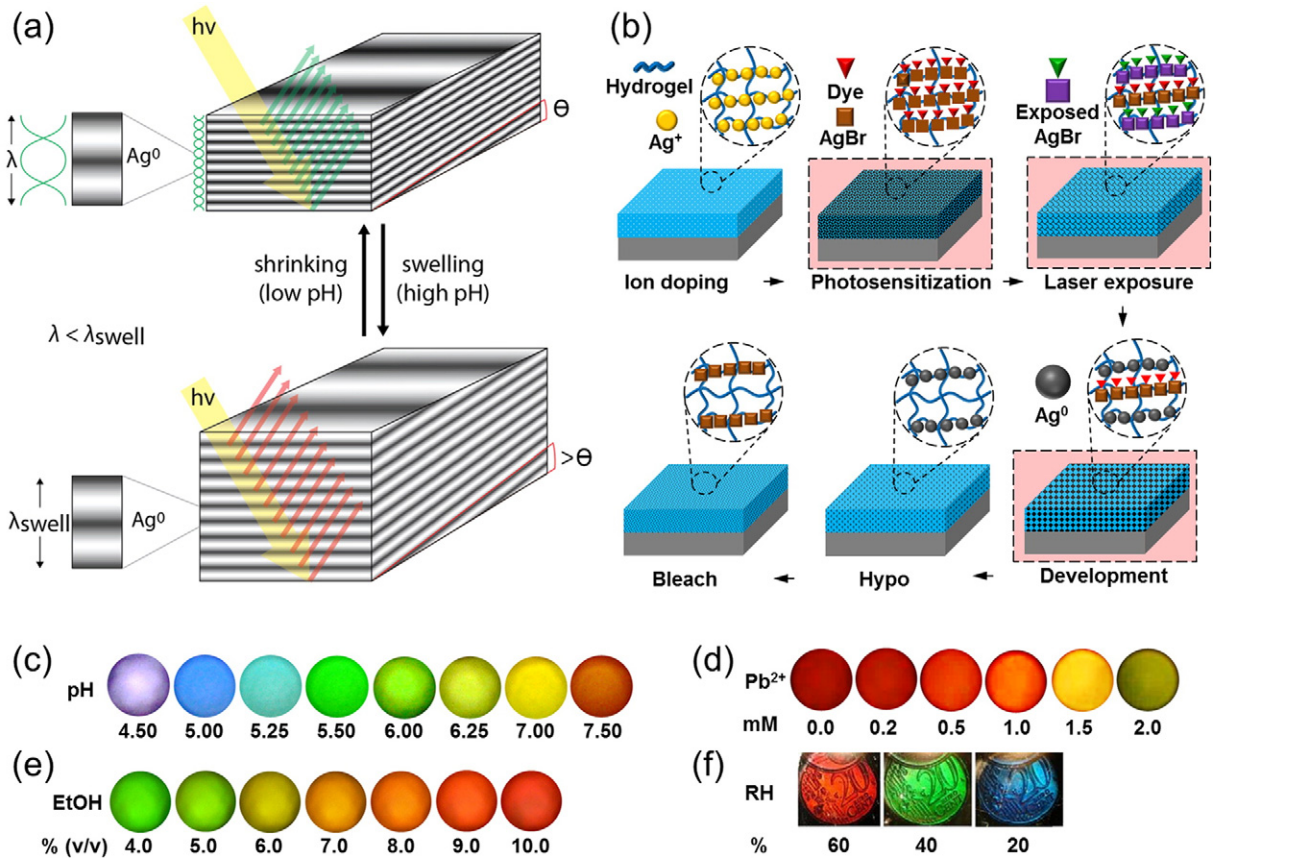

Fig. 1. Holographic sensors. (a) The modulation of Bragg diffraction gratings in reflection holographic sensors as a function of pH. An increase in pH swells the hydrogel matrix and expands the lattice spacing of the grating, shifting the diffracted light to longer wavelengths. (b) Fabrication of holographic sensors by silver halide chemistry and laser writing. (c) Colorimetric response of holographic carboxylated pHEMA pH sensor. Reprinted with permission from Yetisen et al. (2014a). Copyright, Wiley-VCH Verlag GmbH&Co. KGaA, Weinheim. (d) 8-hydroxyquinoline-functionalized Pb^{2+} ions. Reprinted with permission from Yetisen et al. (2015a). Copyright, American Chemical Society. (e) pHEMA ethanol sensor. Reprinted with permission from Yetisen et al. (2014g). Copyright, The Royal Society of Chemistry. (f) Poly(acrylamide-*co*-vinylalcohol) humidity sensor with image displaying capabilities. Reprinted with permission from Naydenova et al. (2008). Copyright, American Institute of Physics.

derivatives (Kabilan et al., 2004; Marshall et al., 2003; Mayes et al., 2002; Yetisen et al., 2014g). Functional groups can also be introduced after polymerization through a *N,N'*-dicyclohexylcarbodiimide (DCC)-initiated condensation reaction by forming amide linkages (Yetisen et al., 2015a). Alternatively, sensitivity to analytes can also be achieved by introducing nanoparticles (zeolites) to the monomer mixture (Leite et al., 2010a,b; Zaarour et al., 2014).

The fabrication of holographic sensors involves forming diffraction gratings in the hydrogel matrix. Depending on the hydrophilicity of the polymer matrix, silver halide chemistry, high-energy laser patterning, or multilayer photopolymerization can be used to record the photonic structure. The early holographic sensors were recorded by silver halide chemistry (Millington et al., 1996). In gelatin emulsions, silver halides are prepared when the gelatin is molten in aqueous conditions, and coated over a substrate as thin film. However, this strategy is not universally applicable due to the immiscibility of some monomer species with water. Hence, a diffusion method was developed for doping hydrogel matrixes with Ag^+ ions (Blyth et al., 1999). Typically, under safelighting, Ag^+ ions are converted to AgBr nanocrystals using aqueous LiBr in the presence of photosensitizers (Marshall et al., 2003). Subsequently, the recording medium is exposed to holographic laser light interference pattern to produce a latent image, which can be later converted to Ag^0 nanoparticles using a photographic developer (Fig. 1b).

Holographic sensors can also be recorded by using intense pulses of laser light (Yetisen et al., 2014e). For example, high-energy frequency doubled Nd:YAG (Nd–Yttrium–Aluminum–Garnet) nanosecond (ns) pulsed lasers or other high-energy lasers can be used to create reflection holograms (Martinez-Hurtado et al., 2010). The typical laser energy output of such lasers is 300 mJ with a pulsed laser operating at 532 nm. However, low-cost Q-switched lasers for tattoo removal can also be used. In contrast to silver halide holography, high-energy patterning does not require formation of silver halide nanocrystals. This fabrication method consists of the impregnation of the hydrogel matrix with a light-absorbing material and highly-intense laser exposure of the recording media to form diffraction gratings. For example, Ag^+ ions can be perfused into the hydrogel matrix, and reduced *in situ* using a photographic developer to Ag^0 nanoparticles (Ø = 50–100 nm). Nanoparticles of this size absorb in a wavelength range overlapping with the laser emission wavelength at 532 nm. Similarly, other metal nanoparticles (*i.e.* gold or iron), pigments, dyes, and carbon nanotubes can be used to produce the gratings (Vasconcellos et al., 2014; Zhao et al., 2015a). The interaction of laser light with nanoparticles might result in reduction of particle size, oxidation, modification in the crystal structure or morphology, further crosslinking, or diffusion in the antinode or node regions, which may contribute to reorganizing the nanoparticles in the hydrogel matrix (Yetisen et al., 2014a).

Holographic sensors can also be constructed using photopolymers (Mikulchyk et al., 2014). A significant advantage of photopolymers over silver halide chemistry and high-energy patterning is the ability to achieve high diffraction efficiency. Photopolymer-based holographic sensors are typically constructed from AAm and VA (Mikulchyk et al., 2013; Naydenova et al., 2008, 2009). To fabricate the hologram, a mixture of monomers, crosslinker, photoinitiator and sensitizers are coated over a substrate. The resulting hydrogel matrix is exposed to an interference pattern to create a multilayer photonic structure. When the light is

absorbed at the antinode regions of the standing wave, the monomers undergo free radical chain polymerization. Hence, this process locally changes the refractive index and the polarization of the molecules. The spatial variation in the intensity of the interference pattern is recorded as a variation of refractive index.

Holographic sensors have been utilized to sense ions, metabolites, enzymes, drugs, microorganisms, and other clinically relevant stimuli (Yetisen et al., 2014f) (Table 1). Earlier research in holographic sensors focused on the development of pH sensors (Marshall et al., 2003). Functionalization with acidic or basic groups allowed the hydrogel matrix to swell and shrink due to the change in Donnan osmotic pressure as the pH of the system was varied (Fig. 1c). The monomers that can be incorporated in holographic pH sensors include methacrylic acid (MAA), trifluoromethyl propenoic acid (TFMPA), dimethylaminoethyl methacrylate (DMAEM), and vinyl imidazole to detect the pH from 2.0 to 9.0 to achieve 0.01 pH unit sensitivity. A limitation of hydrogel-based pH sensors is that they are affected by changes in ionic strength.

Holographic sensors have been utilized in the quantification of mono/divalent metal ions in clinical chemistry. Holographic sensors were functionalized with methacrylated crown ethers to sense K^+ ions (Mayes et al., 2002). A holographic sensor containing 18-crown-6 (50 mol%) allowed sensing K^+ ions (≤30 mM) within 30 s. Recently, porphyrin derivatives were incorporated into holographic sensors for the detection of divalent metal ions (Yetisen et al., 2014g). Holographic sensors consisting of porphyrin derivatives as chelating agents responded to Cu^{2+} and Fe^{2+} ions within the concentration range of 0.05–1.00 mM in 30 s. However, these sensors were insensitive to divalent metal ions below 10 mM (Yetisen, 2015c). The same sensors were also used to sense alcohols as the concentration of ethanol was varied from 4 to 10% (v/v) (Fig. 1d). Another recent holographic sensor featuring 8-hydroxyquinoline (8HQ) as a chelating agent for Pb^{2+} ions was shown to have a dynamic range of 0.1–10.0 mM with a limit of detection of 11.4 μM (Fig. 1e) (Yetisen et al., 2015a). Holographic sensors incorporating boronic acid derivatives were shown to be sensitive to glucose. 3-(acrylamido)phenylboronic acid (3-APB) (pK_a = ~8.8) binds to carbohydrates by forming reversible covalent bonds through its *cis*-diol units (Kabilan et al., 2004, 2005). The principle of operation of the holographic glucose sensors was based on the change in Donnan osmotic pressure, which shifted the Bragg peak to longer wavelengths in the presence of carbohydrates (Yetisen, 2015b).

Holographic sensors also have the capability to incorporate images (Naydenova et al., 2008). Holographic humidity sensors were fabricated in AAm photopolymer in Denisyuk reflection mode (Fig. 1f). After breathing over the holographic sensor, the change in the diffracted light provided a qualitative and quantitative readout of the relative humidity (RH) in the environment. The color change was observed within seconds after changing the RH, and this process was reversible. Additionally, images can be incorporated within holographic sensors that display a different image upon interacting with a target analyte.

2.2. Crystalline colloidal array sensors

Periodic CCAs consisting of microparticles can restrict the propagation of photons within a certain range of wavelengths. In nature, such structures are found in opals, in which amorphous silica particles are periodically arranged. The optical characteristics of the diffracted light from colloidal crystals depend on the particle order, size, and the refractive index of the particles and their surrounding medium. CCAs embedded in hydrogels represent a colorimetric and reversible sensing technology for applications in IVD (Zhao et al., 2010a). CCAs consist of three-dimensionally ordered polystyrene (PS) or poly(methyl methacrylate) (PMMA) particles that self-assemble into a body-centered cubic (BCC) or face-centered cubic (FCC) lattice due to electrostatic repulsion between the monodisperse, highly charged particles. With a mesoscopic periodicity of 0.1–1.0 μm, the CCA forms single crystals that Bragg-diffract visible light (Fig. 2a) (Carlson and Asher, 1984; Rundquist et al., 1989). The diffracted light is monochromatic and can be tuned in the visible spectrum (Fig. 2b).

Table 1
The quantification capabilities of holographic sensors in medical diagnostics.

Stimulus	Recognition group	Dynamic range	Sensitivity	Ref.
Trypsin (μg mL^{-1})	Gelatin degradation	<20	0.04	Millington et al. (1996)
Water content in solvents (ppm)	Matrix interaction	<20,000	120	Blyth et al. (1996)
Alcohol (%)	Matrix interaction	<100	0.3	Mayes et al. (1999)
K^+ ions (mM)	18-crown-6	<30	1	Mayes et al. (2002)
pH	CA	2–9	0.0006	Marshall et al. (2003), Tsangarides et al. (2014), Yetisen et al. (2014a)
Glucose (mM)	Phenylboronic acid	<375	0.09	Domschke et al. (2006), Horgan et al. (2006), Kabilan et al. (2004, 2005), Kraiskii et al. (2010), Lee et al. (2004a), Worsley et al. (2007, 2008), Yang et al. (2006, 2008), Yetisen et al. (2014d)
Ionic strength (mM)	Charged sulphonate and quaternary ammonium	<500	0.08	Marshall et al. (2004b)
Penicillin G (mM)	Penicillinase	<1–25	0.05	Marshall et al. (2004a)
Urea (mM)	Urease	<50	0.15	Marshall et al. (2004a)
Ca^{2+} (μM)	Iminodiacetic acid, nitrilotriacetic acid	<70	2.2	Bhatta et al. (2007), Gonzalez et al. (2005)
Lactate (mM)	Phenylboronic acid	<12	0.1	Sartain et al. (2006, 2008)
Calcium dipicolinate (mM)	Acid-soluble spore proteins	>50	40	Bhatta et al. (2008)
Humidity (%, RH)	Matrix interaction	10–80	1	Naydenova et al. (2008, 2009, 2011)
Edrophonium (μM)	Acetylcholinesterase and CA	<300	0.4	Tan and Lowe (2009)
Alkanes, alkenes, alkynes (% v/v)	Matrix interaction	<100	0.5	Martinez-Hurtado et al. (2010, 2011)
Co^{3+} (mmol l^{-1})	Ionogens	<10	0.1	Kraiskii et al. (2010)
Organic solvents (%, v/v)	Matrix interaction	<10	0.1	Yetisen et al. (2014g)
Testosterone (μM)	Molecular imprinting	<10	1.0	Fuchs et al. (2013, 2014)
Cu^{2+}, Fe^{2+} (1 **M**)	Porphyrins	<1.0	0.1	Yetisen et al. (2014g)
Ammonia (NH_3) (%, v/v)	Nafion	0.19–12.5	2	Hurtado and Lowe (2014)
Pb^{2+}	8-Hydroxyquinoline	0.1–10.0 mM	11.4 μM	Yetisen et al. (2015a)

The synthesis of monodisperse, highly charged PS or PMMA spheres (100 nm) was carried out through emulsion polymerization (Reese et al., 2000) (Fig. 2c). A solution (~8 wt.% colloids) was combined with a monomer mixture and allowed to equilibrate (Fig. 2d). CCAs were then fabricated by the co-polymerization of monodisperse nanoparticles and monomers to immobilize the suspension (Fig. 2e) (Asher et al., 1994). The CCA lattice spacing and subsequent diffracted wavelength could be tuned by varying the concentration of the colloidal nanoparticle solution (Fig. 2f). For example, a change of 0.5% in the hydrogel volume shifted the diffracted peak by ~1 nm (Holtz and Asher, 1997).

By incorporating different recognition sites, CCAs have been used for several applications in IVD. The CCA materials can be functionalized with chelating agents and ligands. Hydrogels consist of greater than 85% water, which allows target analytes to freely diffuse into the CCA matrix to bind to the recognition group with diffusion constants that can be approximated by those in water (Asher et al., 2002). As the recognition group in the hydrogel matrix binds to target analytes, the Donnan osmotic pressure of the hydrogel matrix increases (or decreases) by absorbing more (or less) water. The changes the hydrogel volume is thus directly proportional to the concentration of the target analyte (Holtz and Asher, 1997; Holtz et al., 1998). This volume change shifts the diffracted Bragg peak to longer wavelengths, which can be correlated with the analyte concentration. The color change can be semi-quantitatively interpreted by eye, or quantitatively analyzed using a spectrophotometer. Therefore, CCAs offer a practical and equipment-free approach to IVD that can be used in the field to obtain rapid analyses.

The volume-phase transition of poly(AAm-*co*-CA) CCA in response to pH and ionic strength changes has been monitored (Lee and Asher, 2000). The pH sensor operated from pH 2–11 and shifted the Bragg peak ~ 250 nm. The shift due to Na^+ ions (10 mM) was 200 nm at pH 8.1. A volume-phase model was also developed to predict pH and ionic strength dependence of hydrogel swelling. This enabled the design of materials for optimal pH and ionic strength sensors by using functional groups that ionize in various pH ranges or that show no pH dependent ionization.

Crown ethers were attached to the pAAm CCA hydrogel to selectively bind Pb^{2+} ions (Asher et al., 2002). The measurement of blood lead concentration has diagnostic applicability in plumbism (lead poisoning). The reference range for acceptable blood lead concentration (BLC) is 0.5–1.0 μmol/L (Kratz, 2004). In lead poisoning, BLC exceeds 0.97 mmol/L (Haslam, 2003). Lead encephalopathy, more common in children than adults, is diagnosed at blood lead concentrations from 4.83–14.49 mmol/L (Trope et al., 2001). The immobilization of Pb^{2+} ions in the CCA increased the influx of their counterions, which increased the Donnan osmotic pressure and swelled the hydrogel in proportion to the concentration of bound Pb^{2+} ions (Asher et al., 2002). A red-shifted Bragg diffraction acted as a sensor for quantification of the concentration of Pb^{2+} ions in low ionic strength solutions. However, at high ionic strength, the Donnan osmotic pressure from Pb^{2+} ion chelation was saturated by non-specific interaction with other cations in the solution, and the sensors became ineffective. To overcome this challenge, the CCAs were incubated in a sample solution, and their transient response was measured after rinsing the sensor with pure water. Since the non-complexed counterions diffuse out of the CCA matrix more quickly than the bound Pb^{2+} ions, this transient diffraction shift was proportional to the concentration of Pb^{2+} ions. CCAs sensed Pb^{2+} ions in high ionic-strength environments such as body fluids with a detection limit of 100 ppb. For lead concentrations greater than 10 μM, the CCA color change was visible to the eye. To detect lower concentrations of Pb^{2+} ions in high ionic strength, an optode sensing device was developed (Reese and Asher, 2003). It consisted of a probe assembly containing the CCA sensing material, a diode array spectrometer, and a fiber

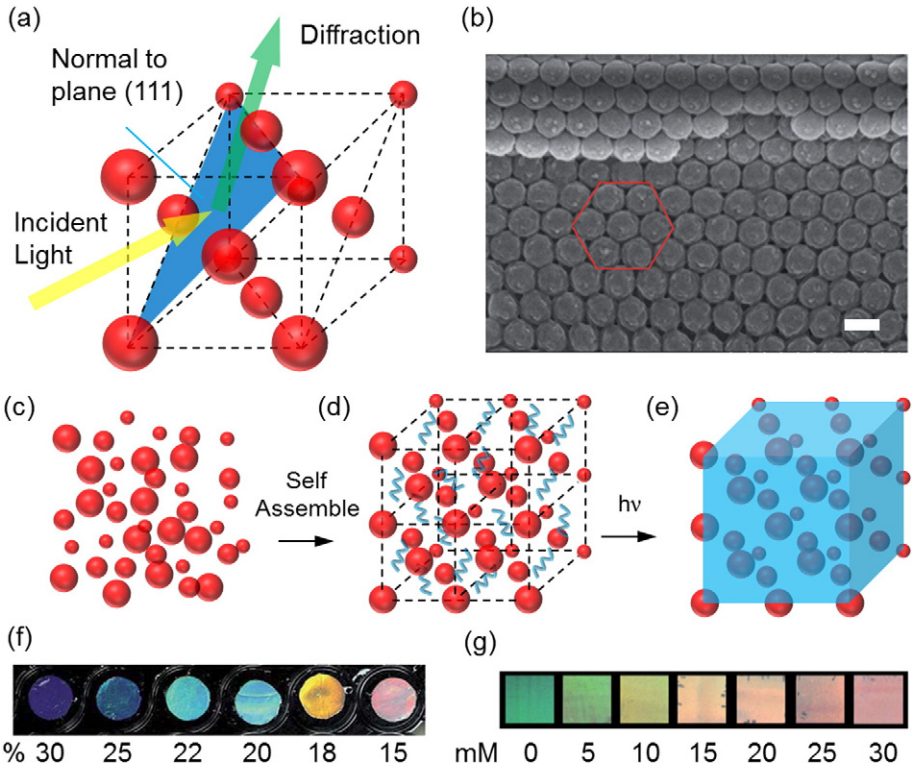

Fig. 2. Crystalline colloidal array (CCA) sensors. (a) The principle of operation that obeys Bragg's law. (b) Scanning electron microscopy image of CCAs showing face centered cubic (FCC) array. Scale bar = 2 μm. Reprinted with permission from Sai et al. (2013). Copyright, the Royal Society of Chemistry. (c) Monodisperse, highly charged PS or PMMA spheres synthesized through emulsion polymerization that (d) undergo electrostatic repulsion and self-assemble to form FCC lattices, with subsequent (e) monomer mixture photopolymerized around the CCA. (f) The diffracted light from CCAs can be tuned in the visible spectrum by changing the concentration of the silica nanoparticles. Reprinted with permission from Ye et al. (2011). Copyright, American Chemical Society. (g) Colorimetric response of molecularly imprinted CCA sensors as the concentration of *p*-nitrophenol was increased from 5 to 30 mM. Reprinted with permission from Xue et al. (2014b). Copyright, The Royal Society of Chemistry.

optic reflectance probe. The optode might allow for the rapid removal of non-complexed ions present in biological samples. Recently, a CCA sensitive to thiocyanate ions (SCN^-) was synthesized (Ma et al., 2013). Polystyrene-co-poly(*N*,*N*-dimethylacrylamide) (PS-*co*-PDMAA) microspheres consisting of PS core and PDMAA shell were prepared by emulsion polymerization (Xiao et al., 2004). To construct the array, 3D self-assembly of a CCA was induced by centrifugation. Consequently, the CCA was tested in a plate groove. As the concentration of SCN^- ions increased from 8.6 to 860 nmol/g, the Bragg peak linearly red-shifted 290 and 60 nm, respectively. The red shifts of other anions (8.6 nmol/g) were greater than 95 nm. While this assay provided broader operational wavelength ranges as compared to the polymerized CCAs, this assay required centrifugation for each experiment.

pAAm CCAs containing creatinine deiminase enzyme and 2-nitrophenol titrating group were used to detect and quantify creatinine, a marker of renal dysfunction, in human blood serum samples (Sharma et al., 2004). When creatinine diffused into the hydrogel matrix, it hydrolyzed by the creatinine deiminase, increasing the local pH, which deprotonated a second recognition agent, 2-nitrophenol. The deprotonated phenolate exhibited enhanced solubility, swelled the hydrogel matrix and red-shifted the Bragg peak. The changes in the Bragg peak position allowed the quantification of creatinine concentration with a physiologically relevant limit of 6 μM (Sharma et al., 2004).

Organophosphorus compounds are potent inhibitors of nervous system function and are used worldwide in agriculture, creating a need for a rapid, low-cost method of their detection (Radic et al., 1993; Dziri et al., 1998). The organophosphorus compound parathion was detected as low as fM using CCA sensors containing acetylcholinesterase (AChE) (Walker and Asher, 2005). AChE bound organophosphorus compounds irreversibly and created anionic phosphonyl species, which increased the Donnan osmotic pressure in the hydrogel matrix that red shifted the Bragg peak. Since the binding was irreversible, the AChE-CCAs acted as dosimeters for parathion.

Elevated concentrations of ammonia in the blood damages the central nervous system and inhibits the generation of postsynaptic potentials (Hazell and Butterworth, 1999; Lockwood, 2004). Routine screening of ammonia blood concentration of at-risk patients is a clinical need that could prevent neurological damage. (Bachmann, 2003). Hyperammonemia is commonly associated with cirrhosis and chronic alcoholism, in which the liver cannot adequately clear out ammonia (Shimamoto et al., 1999). An ammonia sensor that quantified the concentration of ammonia in human blood serum in the physiological range of 50–350 μM was synthesized by binding 3-aminophenol to the poly(hydroxyethyl acrylate) (pHEA) CCA backbone (Kimble et al., 2006). Ammonia reacted with hypochlorite and the pendant aminophenol in the Berthelot reaction to create benzoquinone chlorimine, which reacted with another pendant aminophenol to form a crosslink. The crosslinking of the hydrogel caused the matrix to shrink, and blue-shifted the diffracted light.

Recently, a CCA sensor has been developed to detect enzyme activity by tethering a target peptide (LRRASLG) to the hydrogel matrix as a substrate for protein kinase A (PKA) (MacConaghy et al., 2015). The peptide became phosphorylated by PKA, resulting in additional negative charges in the hydrogel and the creation of a Donnan potential which changed the hydrogel volume and subsequently shifted the Bragg diffraction. By eliminating extraneous charges in the hydrogel through functionalization with azide-alkyne click chemistry, the hydrogels were able to detect phosphorylation in 30 min and had a sensitivity limit of 0.1 U/μL PKA in 2 h (MacConaghy et al., 2015).

The diagnosis and treatment of diabetes also require rapid sensors that can be produced at low-cost, particularly in developing countries. Phenyl boronic acid derivatives form reversible covalent bonds with carbohydrates through *cis*-diols (Hisamitsu et al., 1997; Zhang et al., 2013a). Boronic acid ($pK_a = 8.8$) is in uncharged and trigonal configuration below pH 7.0; however, at pH values greater than its pK_a value, boronic acid is in tetrahedral coordination form (Springsteen and Wang, 2002). The tetrahedral form can bind to *cis*-diols of carbohydrates, resulting in boronate ionization. This binding mechanism has been utilized in CCAs for sensing carbohydrates (Asher et al., 2003). A CCA was synthesized from copolymerization of AAm and boronic acid derivatives. The sensor produced a Bragg peak shift of 60 nm as the concentration of glucose was increased to 10 mM (pH 8.5, 2 mM Tris–HCl buffer). In another study, CCA embedded in phenyl boronic acid derivative functionalized pAAm–poly(ethylene glycol) PEG, and a pAAm-15-crown-5 matrix was utilized to quantify the concentration of glucose in solutions (Alexeev et al., 2003). The complexation of phenyl boronic acids and the *cis*-diols of glucose molecules increased the hydrogel crosslinking, and blue-shifted the Bragg peak. For example, a boronic acid-pAAm-PEG CCA sensor produced a blue Bragg peak shift by 60 nm for 8 mM glucose (pH 8.5, 2 mM Tris–HCl buffer) while the sensor produced a 100 nm shift at pH 9.5 (Fig. 2g) (Alexeev et al., 2003). Table 2 shows the dynamic ranges and sensitivities of CCA sensors.

Molecularly imprinted polymers (MIPs), which have been used in chemical and biological sensors as selective recognition elements with a high affinity for a target molecule, can be used to create receptor sites in CCAs. MIPs contain specific recognition sites that are complementary in size, shape and functional groups to the template molecules and involve an interaction mechanism based on molecular recognition (Wulff, 1995). For example, CCA sensors incorporating MIPs were used for the detection of bisphenol A (BPA), a suspected endocrine-disruptor which adversely affects human growth and development (Guo et al., 2012). Molecularly imprinted monodisperse PMMA nanoparticles were prepared with suspension polymerization, resulting in numerous nanocavities distributed in the PMMA spheres that provided specific recognition sites for BPA. By measuring the change in diffraction intensity corresponding to BPA concentrations, the sensor can detect between 1 ng/mL and 1 g/mL (Guo et al., 2012). Similarly, the combination of MIP and CCA has also been used for the detection of diethylstilbestrol (DES), which has clinical utility in testing the risk of breast cancers and clear cell adenocarcinoma of the cervix (Palmer et al., 2006; Sai et al., 2013). The diffraction efficiency of the CCA decreased in 7 min upon increasing the DES concentration from 2 ng/mL to 8.2 mg/mL with no obvious changes in efficiency for DES analogues (Sai et al., 2013). Furthermore, molecularly imprinted CCAs have been used to measure the concentration of *p*-nitrophenol (Xue et al., 2014b). As the concentration of *p*-nitrophenol was increased to 30 mM, the Bragg peak of the CCA shifted 55 nm to longer wavelengths, showing a detection limit of 1 mM. The color change was visible to the eye (Fig. 2g).

CCAs that can maintain their color independent of the observation angle have been synthesized (Yeo et al., 2015). Monodisperse double emulsions encapsulating CCAs were prepared using a microfluidic device. Inducing crystallization of highly-charged PS particles in the core of double emulsions through osmotic annealing allowed creating CCAs with improved angle tolerance. This approach also enabled tuning the shape and crystallinity of the CCA supraparticles. These supraparticles were subsequently fixed in an elastomeric matrix. However, this approach produced broadband Bragg diffraction at low diffraction efficiency, limiting the practicality for sensing applications. Recently, CCAs with uniform, Janus, multicomponent, or core-shell inner structures have been reported (Zhao et al., 2010b, 2014). The spherical symmetry of such “bead-shaped” CCAs enables their PBGs to be independent of the rotation angle under illumination of the surface at a fixed incident angle. Hydrogel DNA-responsive photonic beads were used for a label-free DNA detection (Zhao et al., 2010c). The hybridization of target DNA and the crosslinked single-stranded DNA shrank the hydrogel and blue shifted the Bragg diffraction peak.

Defects have been introduced to CCA as recognition sites by controlling the population and arrangement of nanoparticles through the creation of gaps, points, lines, planes, and grain boundaries (Arsenault et al., 2006). Such defects allowed for engineered functionality for integrated

Table 2
Crystalline colloidal array sensors.

Stimulus	Recognition group	Dynamic range	Sensitivity	Ref.
Pb^{2+} ions	18-crown-6	<7.5 mM	0.5 μmol/L	Asher et al. (2002)
Urea	Urease	0.05 mM–0.5 mM	N/A	Zeng et al. (2002)
Glucose	Phenylboronic acid	<30 mM	50 μM	Asher et al. (2003), Zhang et al., (2013a)
Creatinine	Creatinine deiminase	<1 mM	0.01 mM	Sharma et al. (2004)
Temperature	Poly(*N*-isopropylacrylamide)	25–40	N/A	Lyon et al. (2004)
Parathion	Acetylcholinesterase	<42.6 pM	4.26 fM	Walker and Asher (2005)
Ammonia	Berthelot reaction	50–300 μM	50 μM	Kimble et al. (2006)
Ethanol	Matrix interaction	<100% (v/v)	N/A	Chen et al. (2011)
Hg^{2+} ions	Urease–urea hydrolysis	<20 ppb	1 ppb	Arunbabu et al. (2011)
Bisphenol A	Imprinted cavity	<1 μg/mL	1 ng/mL	Guo et al. (2012)
pH	Matrix interaction	2.8–9.5 units	0.05 units	Jiang et al. (2012)
Cu^{2+}, Ni^{2+}, Zn^{2+} ions	8-hydroxyquinoline	<1.6 μM	0.08	Jiang et al. (2012)
Cd^{2+} ions	Thiourea	<10 mM	0.01 mM	Lin and Yu (2012)
Avidin	Biotin	1 mg/mL	580 nm/(mg mL^{-1})	Zhang et al. (2013b)
Diethylstilbestrol	Imprinted cavity	2 ng mL^{-1}–8 μg mL^{-1}	N/A	Sai et al. (2013)
Protein kinase A	Peptide LRRASLG	10 U/μL	0.1 U/μL	MacConaghy et al. (2015)

optics. For example, creation of a single row of missing spheres in a CCA provided a path for light guiding through the periodic lattice. Additionally, a bend was created in the waveguide on the order of the wavelength of the light and a bend radius on the order of one particle diameter. This approach enabled the creation of miniaturized circuit patterns that might find application in integrated optics and sensors. Defects in CCA could be introduced by photolithography, direct writing in confocal microscopy, and high-energy beam surface writing. Air core waveguides were constructed in silicon inverse opals by inserting linear air cavities in the interior of a lattice of silica spheres (Vekris et al., 2005). This process involved photolithographically printing a pattern of photoresist lines on the colloidal surface, and then depositing silica spheres to cover the photoresist layer. Next, this layer was removed to create a pattern of linear air cavities in the CCA. Advanced projection lithography achieved a resolution on the order of 250 nm. Direct writing by laser confocal microscopy involved infiltrating a CCA with a monomer solution, and then scanning the focal volume through the interior of the CCA to locally polymerize the monomer solution. The unpolymerized monomer solution was then removed from the system to leave a polymeric defect in the CCA (Lee et al., 2002; Pruzinsky and Braun, 2005). Linear polymeric patterns with a linewidth on the order of 2 μm at a depth of 0.5 μm were achieved. High-energy beam writing of linear patterns on the surfaces of CCAs have also been demonstrated (Tétreault et al., 2006). This process involved direct writing of laser or e-beam across the surface of the CCA to selectively remove material or induce physical changes. For example, ion lasers were used to change the local recrystallization of amorphous Si to nanocrystalline Si. This process reduced the refractive index of the material from 4.0 to 3.6. Furthermore, irradiation of PMMA spheres with e-beam cleaved bonds to cause solubility in an organic solvent (Ferrand et al., 2003). Subsequently, the exposed materials were removed in a development step to create structural changes.

Planar defects in CCAs can serve as optical dopants that decrease the intensity of Bragg peak at specific wavelengths associated with pseudogap frequencies. The wavelength of defect states within the pseudogap depends on the thickness of the dielectric slab, and its refractive index (Tétreault et al., 2004). A 2D defect consisting of a monolayer of spheres sandwiched between two opal layers with different diameters were created by the Langmuir–Blodgett technique (Egen et al., 2003; Massé et al., 2006; Zhao et al., 2003). Such defects have also been introduced by spin coating spheres or nanocrystalline aggregates in CCAs (Pozas et al., 2006). Furthermore, chemical vapor deposition (Palacios-Lidón et al., 2004; Tétreault et al., 2004) and polyelectrolyte multilayers (Fleischhaker et al., 2005a) have been used to introduce these defects. Polyelectrolyte multilayers were incorporated in photonic crystals by layer-by-layer deposition or transferring the layer over the surface of the photonic structure by using a PDMS stamp, followed by growing a layer of CCA on top of the embedded structural defect. These polyelectrolyte defect layers were functionalized with photochemically active azobenzene polyelectrolytes and redox-active polyferrocenylsilane (PFS) metallopolyelectrolytes. The polyelectrolyte incorporating azobenzene was modulated based on photochemical trans-cis isomerization and thermal back-isomerization of the azo group (Fleischhaker et al., 2005a). The defect transmission state of the redox active polyferrocenylsilane was modulated by oxidizing and reducing the ferrocene units (Fleischhaker et al., 2005b). The polyelectrolyte layers might allow the incorporation of dyes, quantum dots, colloids, and biopolymers such as proteins and DNA (Schönhoff, 2003). For example, CCAs were designed with planar polyelectrolyte defects that incorporated DNA and polypeptides (Fleischhaker et al., 2006). These sensors were used to monitor DNA conformational changes and the enantioselective intercalation of daunorubicin.

2.3. Inverse opal sensors

Inverse opals are constructed by templating monodisperse spheres, typically consisting of silica, PS, PMMA, or block co-polymers (Aguirre et al., 2010). Close-packed arrays from suspended particles can be obtained through centrifugation, sedimentation, vertical deposition, and physical confinement in hydrogels (Furumi et al., 2010; Xia et al., 2000). These close-packed arrays serve as a template that allows infiltration, and the spheres are removed from the medium by pyrolysis and etching (Fig. 3). Inverse opals can be constructed in hydrogel matrixes that are functionalized with covalently linked chelating agents or ligands that can specifically bind to target analytes. Such interactions change the lattice spacing and the refractive index of the interstitial spaces and the hydrogel medium. The physical changes in the hydrogel matrix can be read through the diffracted or transmitted light.

PNIPAAm is a widely studied thermosensitive hydrogel that becomes hydrophobic at 32 °C by undergoing a phase transition from swollen to dehydrated state (Schild, 1992). An inverse opal PNIPAAm film was used as an optical filter by varying the temperature, which shifted the position of the Bragg peak and/or its intensity (Ueno et al., 2007). The thermosensor was prepared by copolymerizing NIPAAm, and MAA. As the temperature was increased from 16 to 31 °C, the Bragg peak of the poly(NIPAAm-*co*-CA) matrix decreased from 660 to 340 nm (Fig. 3d). The shift to shorter wavelengths originated from the shrinkage of the hydrogel matrix, which decreased the FCC lattice spacing. Another inverse opal temperature- and cation-sensitive sensor was templated from a silica sphere array by copolymerizing NIPAAm, *N*,*N*-methylenebisacrylamide, and 4-vinylbenzo-18-crown-6 (Saito et al., 2003). At 36 °C, K^+ ions (40 mM) shifted the Bragg peak 200 nm to longer wavelengths (Fig. 3e). However, the sensor was also sensitive to changes in ionic strength. The color range of inverse opal hydrogels

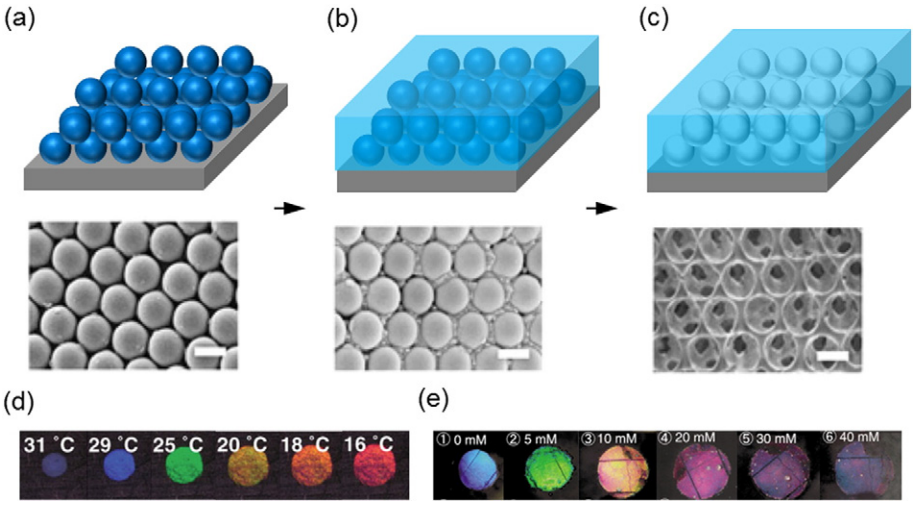

Fig. 3. Inverse opal sensors. (a) The fabrication of inverse opal structure by the self-assembly of a colloidal crystal template, (b) infiltration by a monomer mixture, polymerization, and (c) the removal of colloidal crystal template, scale bars = 500 nm. Reprinted with permission from Kim et al. (2013), Copyright, Macmillan Publishers Ltd. (d) PNIPAAm-*co*-CA thermosensors. Reprinted with permission from Ueno et al. (2007), Copyright, Wiley-VCH Verlag GmbH&Co. KGaA, Weinheim. (e) PNIPAAm-*co*-4-vinylbenzo-18-crown-6 K^+ ion sensor. Reprinted with permission from Saito et al. (2003), Copyright, The Royal Society of Chemistry.

can be tuned by controlling the concentration of the crosslinker and the size of the templating spheres (Takeoka and Watanabe, 2003; Takeoka et al., 2003). Humidity-sensitive pAAm inverse opals were also developed (Barry and Wiltzius, 2006). When the relative humidity was changed from 20 to 80%, the Bragg peak red shifted from 538 to 580 nm. Recently, humidity-sensitive silk-fibroin inverse opals were developed (Diao et al., 2013). The humidity-induced cyclic contraction of silk fibroin enabled continuous modulation of the diffracted color. pH-sensitive inverse opal hydrogels were also synthesized from HEMA and acrylic acid (AA) (Lee and Braun, 2003). The range of Bragg peak shift was controlled by changing the concentration of the AA and the crosslinker. The peak red shifted 300 nm as the pH was increased from 4 to 7, showing a sensitivity of 0.01 pH units.

Inverse opals have been utilized to sense clinically-relevant analytes. Glucose-sensitive inverse opals were synthesized in pHEMA matrixes containing 3-APB (Lee et al., 2004b). Phenylboronic acid reversibly binds to 1,2-*cis* diols such as glucose, which increases the degree of ionization. This swells the hydrogel matrix by an influx of water and ions, and subsequently red shifts the Bragg peak. Inverse opals were optimized to respond to concentrations within the clinical range (<7.0–15.0 mM) of glucose in blood to indicate hyperglycemia (Nakayama et al., 2003). The diffracted light shifted from green to yellow/orange to red as the concentration of glucose was changed from 5.0 to 10.0 to 15.0 mM. In another study, inverse opals were used to sense alcohols (Pan et al., 2012). A single crystalline inverse opal hydrogel was fabricated by PS opal templating in pAAm. Its diffraction spectra changed from about 640 to 450 nm when the alcohol (methanol, ethanol, or *n*-propanol) concentration was increased. This sensor was also responsive to the variation in the concentration of PEG. Inverse opals have also been used to detect ammonia (Liu et al., 2012). TiO_2 inverse opals were fabricated by infiltration with polyaniline. The sensor changed its color from red to green reversibly in response to ammonia. This change was observed by eye, which may have clinical utility for monitoring ammonia vapor, such as from breath (Shimamoto et al., 1999). Furthermore, dimethyl aminopropyl methacrylamide was incorporated in inverse opals as a functional monomer to sense CO_2 (Hong et al., 2013). After exposure to CO_2, the tertiary amine groups in this monomer were protonated and formed ion pairs with CO_2. This swelled the hydrogel matrix and red shifted the diffracted light. Non-invasive CO_2 sensors could have applications in monitoring of respiratory physiology and pathologies (Folke et al., 2003). Table 3 shows the inverse opal sensors and their detection capabilities.

2D monolayer inverse opal hydrogels are promising candidates for sensing, and they have a number of advantages over 3D inverse opal hydrogels (Li and Lotsch, 2012; Xue et al., 2014a). Their advantages include (i) faster and simpler formation of the 2D array template through self-assembly, (ii) a more stable ordering of the 2D array template, which makes it easier to introduce the monomer solution into the template, and (iii) the optical characterization that can be achieved by analyzing Debye diffraction ring (Tikhonov et al., 2012).

2.4. Porous silicon sensors

Photonic biosensors have been fabricated from porous silicon (DeLouise et al., 2005). A single crystal silicon wafer was electrochemically etched using hydrofluoric acid. The diameter (20–150 nm) and morphology of pores in n-type silicon were controlled by changing the etch parameters such as doping level, current density, and electrolytes. The resulting structures acted as Bragg gratings that could be tuned from visible to near-infrared regions of spectrum. Hydrogel-supported membranes were fabricated by either laminating the structure with a crosslinked hydrogel or depositing a monomer solution over the pores prior to crosslinking. Functionalizing the internal surface of the pores by bio-receptors and hydrogels allowed changing the position of the Bragg peak, which was correlated with concentration values of a target analyte. For example, pAAm was functionalized with amine groups and was incorporated into the porous silicon. Changes in the effective refractive index of disulfide crosslinked hydrogel in porous silicon were monitored upon exposure to tris(2-carboxyethyl) phosphine (TCEP). After submerging the photonic silicon in TCEP (50 mM) for 15 min and drying for 5 min, the reflectance peak shifted ~100 nm to shorter wavelengths, producing visible color changes. (Bonanno and DeLouise, 2010). For detecting biomarkers in whole blood, amine-terminated porous silicon surface was functionalized with sulfosuccinimidyl-6-(biotinamido)-6-hexanamido hexanoate, and the sensor response was tested with biotinylated anti-rabbit IgG from goat (Bonanno and DeLouise, 2007). An increase in the concentration of IgG from 1 to 10 mg mL^{-1} produced ~3.3 nm wavelength shift. Additionally, this approach offered intrinsic size-exclusion filtering of erythrocytes, which enhanced signal differentiation.

2.5. Block copolymer sensors

Block copolymers consist of two or more chemically distinct macromolecules that are joined together by covalent or non-covalent bonds

Table 3
Inverse opal sensors and their detection capabilities.

Stimulus	Recognition group	Dynamic range	Sensitivity	Ref.
pH	CA	2–7	0.01	Lee and Braun (2003), Xue et al. (2014a)
Glucose	Phenylboronic acid	<100 mM	0.l mM	Lee et al. (2004b), Nakayama et al., (2003)
Relative humidity	Matrix interaction	20–80%	1–10%	Barry and Wiltzius (2006), Diao et al. (2013)
Temperature	Matrix interaction	16–31 °C	2 °C	Ueno et al. (2007)
Bisphenol A	Molecular imprinting	10^{-8}–1 μM	10^{-9} μM	Griffete et al. (2012)
Cyanide	Trifluoroacetyl	<1 mM	10^{-4} mM	Li et al. (2012)
3-Pyridinecarboxamide	Molecular imprinting	<10 wt.%	0.5 wt.%	Yuan et al. (2012)
PEG in 2-propanol	Matrix interaction	0–90 wt.%	10 wt.%	Pan et al. (2012)
Ethanol, methanol, *n*-propanol	Matrix interaction	0–90 vol%	10 vol%	Pan et al. (2012)
Ammonia	Polyaniline	1–4 (min)	30 nm/min	Liu et al. (2012)
Glucose	Glucose oxidase	1–12 mM	0.5 mM	Jin et al. (2012)
Cholesterol	Molecular imprinting	1 nM–10 μM	1 nM	Zeng et al. (2012)
Cu^{2+} ions	4-Vinylpyridine	N/A	50 mM	Hong et al. (2012)
CO_2	Amino groups	0–4.9 vol%	1 vol%	Hong et al. (2013)
Acetate	Thiourea	10 mM	1 mM	Kado et al. (2013)
Ammonia	Matrix interaction	<100 vol%	N/A	Zhong et al. (2013)
Refractive index	Gold nanoparticles	1.33–1.40	166 nm/RI unit	Cai et al. (2013)
Organic solvents	Matrix interaction	100 vol%	N/A	Cui et al. (2014)
Hg^{2+} ions	CA	10–1000 μM	10 nM	Zhang et al. (2014)
Avidin	Biotin	75–10,000 nM	0.01 nm/nM	Couturier et al. (2015)

(Lynd et al., 2008; Kim et al., 2010). The blocks can be linear chains of identical monomers or branched sequences of monomers. When the blocks are physically incompatible, different macromolecules are thermodynamically driven to self-assemble to reduce the contact between two immiscible regions (Fredrickson and Bates, 1996). Immiscible block copolymers undergo a microphase segregation to form nanostructures with dimensions ranging from 5 to 200 nm, and the control over this process allows tuning of their physical properties and morphology (Bockstaller et al., 2005; Klinger et al., 2013). Thermodynamically incompatible homopolymers phase separate to minimize the enthalpy of the system. However, in block copolymers, entropic forces from the covalent linkages counterbalance the thermodynamic forces driving separation (Bates and Fredrickson, 2008). In contrast to the macrophase separation, the mobility of the copolymer is restricted locally due to the covalent bonding in block copolymers. Unfavorable monomer contacts and the tendency to minimize chain stretching locally segregate layers (Bockstaller et al., 2005). The phase behavior depends on three main factors: degree of polymerization, Flory-Huggins interaction parameter, and the volume fraction of the block (Fredrickson and Bates, 1996). Using block copolymers, 1-3D morphologies with different periodic lattice configurations can be achieved to create optical gratings (Bates and Fredrickson, 1990; Matsen and Bates, 1996). The polymer type, molecular weight, interaction parameter and processing conditions such as the degree of polymerization determines the morphology, such as lamellae, gyroid, cylindrical, or spherical (Fig. 4a) (Hadziioannou and Skoulios, 1982).

Diblock copolymers have been used to construct Bragg gratings by solvent casting polystyrene-block-poly(ethylene/propylene) (PS-b-PE/P) (400 kg/mol) with a polymer dispersion index of 1.04 (Bockstaller et al., 2001). This process created a periodic lamella structure with a spacing of 200 nm. When illuminated with a white light source, the Bragg grating diffracted light at 545 nm. Optical gratings can also be prepared by mixing diblock copolymers with its constituent homopolymers to swell the lamellar microdomains (Urbas et al., 1999). The diblock copolymer/homopolymer allows tailorable lattice spacings, and the use of low molecular weight components. However, the production of optical gratings by self-assembly is limited due to incorrect size of domains needed for the optical ranges of interest, attainment of long-range order, and field of view, or low diffraction efficiency (Edrington et al., 2001). The intrinsic dielectric contrast between the phases in block copolymer-based diffraction gratings is low, which limits the bandgap achievable by block copolymer-based Bragg gratings (Fink et al., 1999). For example, the refractive index contrast between two phases of polystyrene-block-polyisoprene is 1.1. To improve the dielectric contrast, the microdomains of diblock copolymers were doped with nanoparticles (Bockstaller et al., 2001; Chiu et al., 2005, 2007). The surface of nanoparticles can be functionalized to induce affinity to one of the phases of the block copolymer. For instance, PS-coated Au^0 nanoparticles with thiol-terminated ligands were synthesized by the reduction of $HAuCl_4 \cdot 3H_2O$ in THF or two phase liquid system (Brust et al., 1994; Yee et al., 1999). Another challenge with diblock copolymers is that their absorption masks the diffraction within the visible spectrum. Hence, the practical short wavelength limit of diblock copolymers is ~300 nm since such systems have strong absorption in the UV region (Urbas et al., 2002). Furthermore, self-assembled lamellae contain imperfections due to local phase separations and inconsistent orientation of the localized lamellar geometries in symmetric diblock copolymers (Edrington et al., 2001).

The diblock copolymer gratings have been functionalized to render chemical-sensing capability. Polystyrene-*b*-quaternized poly(2-vinyl pyridine) (PS-*b*-QP2VP) lamellar films were synthesized in a few steps. PS-*b*-QP2VP (5% wt, $M_n = 190$ kg mol^{-1}-*b*-190 kg mol^{-1}) in propylene glycol monomethyl ether acetate was spin-casted over a substrate, followed by annealing the matrix in chloroform vapor (50 °C, 24 h) to form in-plane oriented lamellar films (Kang et al., 2007). Subsequently, P2VP blocks were quaternized and crosslinked using a mixture of bromoethane and 1,4-dibromobutane (DBB) in hexane at (50 °C for 24 h). This process converted pyridine to pyridinium in the system. The resulting structure contained a microdomain periodicity of 100 nm with a matrix thickness of 1–3 μm (Fig. 4b). When submerged into an aqueous solution, the thickness of the diblock copolymer matrix expanded to 15–20 μm.

Block copolymers can consist of polystyrene-block-polyacrylic acid (PS-b-PAA), which comprises a hydrophobic PS block and pH-sensitive hydrophilic PAA block. When illuminated with a white light source, block copolymer sensors operate through the modulation of their lattice spacing, and hence shifting the Bragg peak to shorter or longer wavelengths (Fig. 4c). The degree of swelling of the hydrogel matrix can be controlled by the density of crosslinking. Highly-crosslinked regions of the block copolymer were blue and less-crosslinked regions were red in water (Fig. 4d). This block copolymer matrix was used to non-specifically measure ionic strength in water (Kang et al., 2007). When different anions are introduced to the block copolymer matrix, the lamellar structure expanded or shrank depending on the hydration characteristics of each counterion (Lim et al., 2012). Another block copolymer matrix quaternized for 36 h with direct exchange of

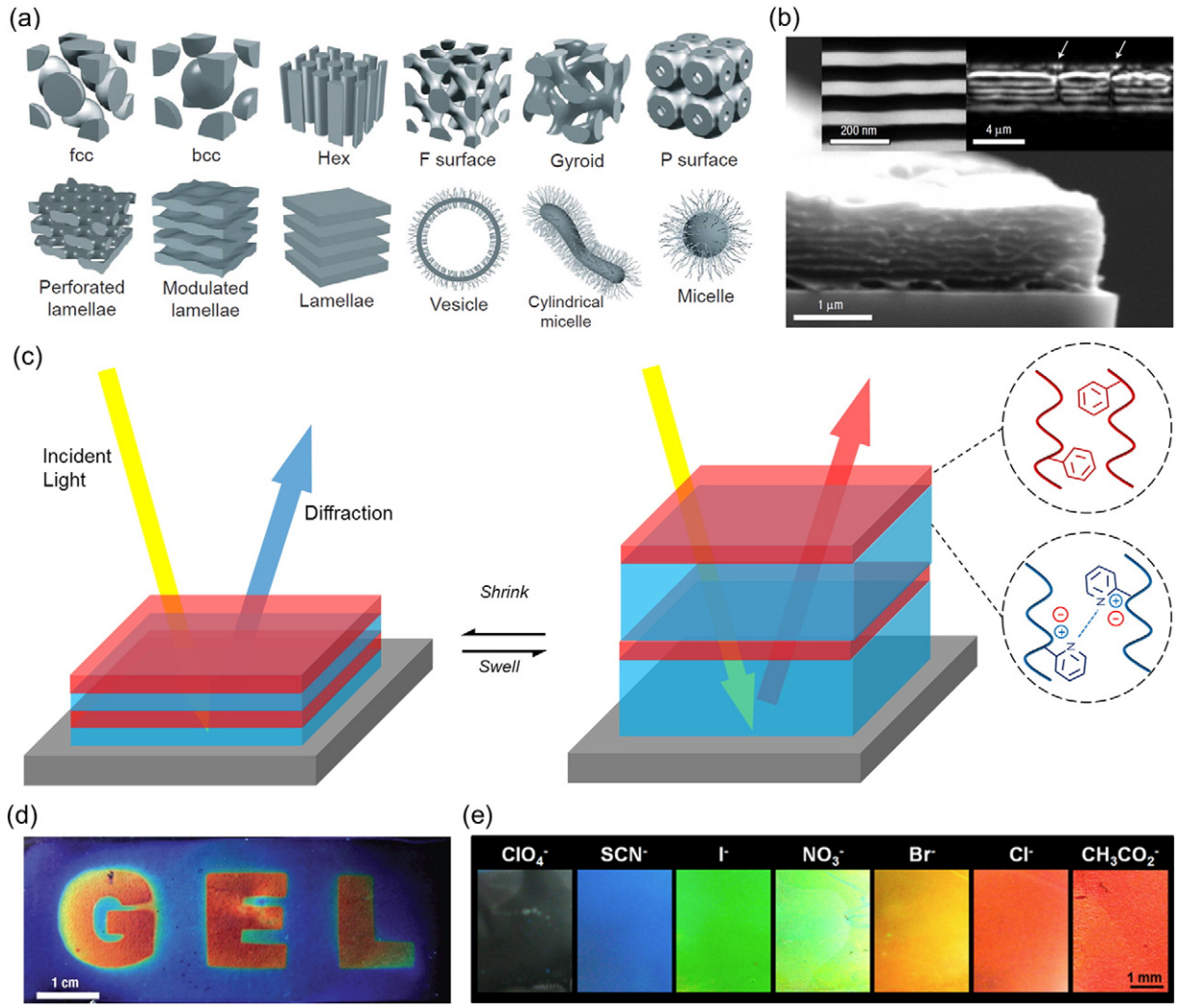

Fig. 4. Block copolymer sensors. (a) Possible self-assembly architectures due to microphase separation. Reprinted with permission from Bucknall and Anderson (2003), Copyright, American Association for the Advancement of Science. (b) SEM micrograph of a PS-b-QP2VP block copolymer film deposited on a silicon wafer. Reprinted with permission from Kang et al. (2007), Copyright, Macmillan Publishers Ltd. (c) The principle of operation. The block-copolymer stack has alternating rigid layers (red) and dynamic polyelectrolyte layers (blue). (d) The degree of crosslinking allows tuning the diffracted light in aqueous solutions. Red regions have lower crosslinking density as compared to blue regions. Reprinted with permission from Kang et al. (2007), Copyright, Macmillan Publishers Ltd. (e) Color change of the block copolymer films quaternized with direct exchange of counteranions. Reprinted with permission from Lim et al. (2012), Copyright, American Chemical Society.

counteranions (10 mM) produced a color change in the visible spectrum (Fig. 4e). In another study, temperature-sensitive block copolymers composed of high molecular weight poly(styrene-*b*-isoprene) (PS-*b*-PI) were anionically synthesized with styrene and isoprene monomers in cyclohexane and benzene (Yoon et al., 2008). The resulting block copolymer matrix was sensitive to temperature changes (30–140 °C). Additionally, phenyl boronic acid derivatives were incorporated in block copolymers to sense carbohydrates (Ayyub et al., 2013). PS-*b*-P2VP functionalized with 2-(bromomethyl)phenylboronic acid quantified the concentrations of fructose up to 50 mM with a detection limit of 0.5 mM. Although the self-assembly of block copolymers is a feasible method in creating multilayer Bragg gratings, it is limited by the requirement of synthesizing high molecular weight block copolymers for sensing applications.

The external shape and internal morphology of block copolymers (*e.g.*, poly(styrene-block-4-vinylpyridine) (PS-*b*-P4VP)) have been controlled by positioning of gold nanoparticle surfactants to create convex patterns (Ku et al., 2014). The assembly of the gold NPs was localized at the interface between P4VP domain at the particles' surface and the surrounding water. This created a balanced interfacial interaction between PS and P4VP domains of the block copolymer to form convex lenses.

2.6. Bragg stack sensors

Bragg stacks consist of alternating layers of high- and low-refractive index materials that upon interacting with incident light produce a strong coloration due to PBG. When the grating is illuminated with a white light source, the light is diffracted from each layer interface, creating narrow-band peaks. Such structures can be rationally designed by changing the film architecture, materials, and the periodicity to obtain desired optical characteristics. For example, the thickness can be varied by spin coating from 10 to 500 nm by controlling spinning speed, withdrawal rate, and the concentration of the deposited solution. Furthermore, the refractive index can be changed by modifying the composition of the deposited materials and porosity. In bottom-up approaches, high- and low refractive index materials such as TiO_2 ($n = \sim 2.85$) and SiO_2 ($n = \sim 1.44$) can be used to construct multilayers (5–10). Many

inorganic materials can be used to construct the Bragg stacks: metal oxides, zeolites, clays, metal-organic frameworks, metals, and semiconductors (Lotsch et al., 2009; Hinterholzinger et al., 2012; Bonifacio et al., 2009).

Hydrogel-based Bragg stacks were constructed from a combination of TiO_2 nanoparticles, and hydrophobic and hydrophilic polymers such PMMA-*co*-pHEMA-*co*-PEGDMA for application in sensing (Wang et al., 2011). Fig. 5a,b illustrates the principle of operation of Bragg stack sensors by increasing the thickness or changing the effective refractive index of the porous layer to induce a shift in Bragg peak. In the presence of solvents, the Bragg peak shifted to longer wavelengths. The initial peak position of the Bragg stack sensors was tuned by changing the hydrogel-TiO_2 ratio during spin coating (Fig. 5c–e). The Bragg stack sensors were tested in the presence of various organic solvents, where each solvent produced a different wavelength shift in the diffracted light (Fig. 5f). For example, the shifts for ethanol and DMSO were 60 and 420 nm, respectively. Another study reported a Bragg stack temperature sensor fabricated by coating high- and low- refractive index photocrosslinkable copolymers: poly(paramethyl styrene) and PNIPAAm (Chiappelli and Hayward, 2012). As the temperature was increased from 20 to 50 °C in water, the Bragg peak blue shifted 300 nm, producing a visible color change (Fig. 5g). The fabrication of Bragg stacks with spin coating has a number of limitations. Spin coating is a multistep process consisting of drying and annealing steps between subsequent layers (von Freymann et al., 2013). Additionally, Bragg stacks are angle dependent; hence, their color changes are based on the position of observation (Bonifacio et al., 2009). The fabrication of organic–inorganic Bragg stacks is limited due to the instability of the polymer in the presence of inorganic sol (colloidal suspension). For example, the inorganic material solution containing TiO_2 sol is acidic, which distorts the morphological integrity of the sublayer (von Freymann et al., 2013).

Layer-by-layer assembly is another approach to create Bragg gratings. It was first introduced for creating structured thin films in biotechnology applications (Decher et al., 1992). The surfaces of many materials including glasses, silicons, and metals carry net negative charges in aqueous solutions due to surface oxidation and hydrolysis. When these planar or curved surfaces are immersed in positively charged polyelectrolyte solutions and rinsed with water, the net charge on the surface becomes positive since polyelectrolytes are absorbed and deposited over the negatively charged surface. Positively charged polyelectrolytes include poly(diallyldimethylammonium chloride) (PDDA), poly(allylamine hydrochloride) (PAH), and polyethyleneimine (PEI). Negatively charged polyelectrolyte solutions can be deposited over the positively charged polyelectrolyte layer, and these steps can be repeated until reaching a desired thickness (Fig. 5h). The water rinsing step is required to remove unabsorbed polyelectrolytes from the surface. Negative polyelectrolytes include poly(styrene sulfonate) (PSS), poly(vinyl sulfate), or PAA. This process builds alternating polyelectrolyte bilayers on the substrate. Layer-by-layer assembly has an accuracy of 1 nm allowing nanoscale control of film thickness (Decher, 1997; Decher and Hong, 1991). While these self-assembly techniques are typically based on electrostatic interactions, polymer bilayers can also be constructed by using hydrogen and covalent bonding (Brynda and Houska, 1996; Sun et al., 1998), hydrophobic interactions (Kotov, 1999; Lojou and Bianco, 2004), charge transfer (Shimazaki et al., 1997), and biological recognition (Anzai et al., 1999). In addition to polyelectrolytes, charged species of layer-by-layer bilayers may include

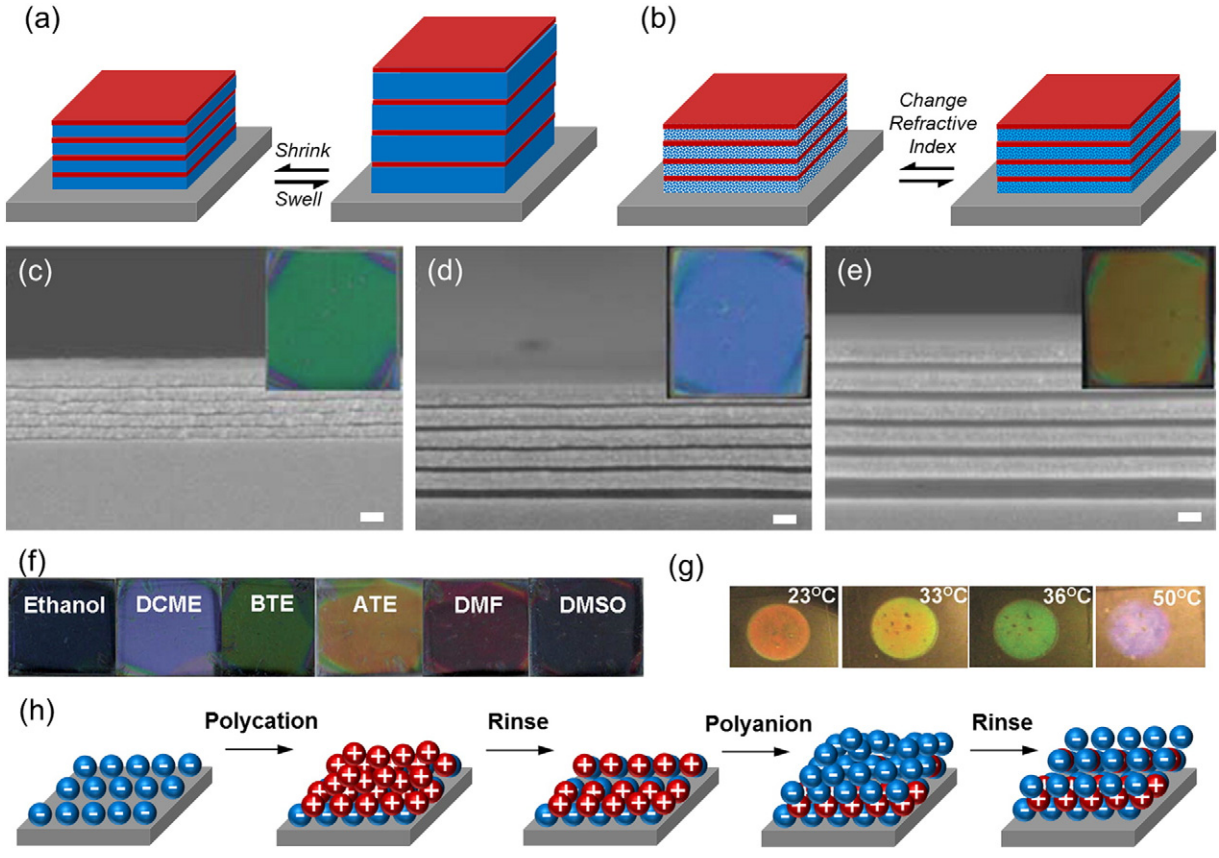

Fig. 5. Bragg stack sensors. Principle of operation by (a) hydrogel swelling, and (b) change of the effective refractive index. (c–e) SEM images of cross-sections of spincoated Bragg stacks consisting of TiO_2 and PMMA-*co*-pHEMA-*co*-PEGDMA with layer thicknesses of (c) 70 and 9 nm, (d) 80 and 20 nm, and (e) 89 and 57 nm. The insets show the diffraction at 2.0 × 2.0 cm. Scale bars = 100 nm. (f) The colorimetric response of spincoated Bragg stacks to organic solvents. (c–f) Reprinted with permission from Wang et al. (2011), Copyright, The Royal Society of Chemistry. (g) Colorimetric readouts of a poly(para-methyl styrene)-PNIPAAm Bragg stack temperature sensor in water. Reprinted with permission from Chiappelli and Hayward (2012), Copyright, Wiley-VCH Verlag GmbH&Co. KGaA, Weinheim. (h) Layer-by-layer assembly of Bragg stack sensors through coating of polyanions and polycations on a negatively-charged substrate.

carbon tubes (Mamedov et al., 2002; Jiang et al., 2005), nanoparticles (Kotov et al., 1995), nanoplates (Keller et al., 1994; Kleinfeld and Ferguson, 1994), organic dyes (Cooper et al., 1995), porphyrins (Araki et al., 1996), dendrimers (He et al., 1999), polyoxometalates (Ingersoll et al., 1994; Liu et al., 2003), polysaccharides (Lvov et al., 1998; Richert et al., 2002), polypeptides (Müller, 2001; Boulmedais et al., 2003), proteins (Hong et al., 1993; Kong et al., 1994; Lvov et al., 1994, 1995), DNA and nucleic acids (Lvov et al., 1993), and viruses (Yoo et al., 2006). In sensing applications, PAA/PAH and PAA/poly(sodium 4-styrenesulfonate) (SPS) layers reversibly responded to pH and organic solvents (Zhai et al., 2004). A limitation of layer-by-layer assembly is time consuming polyelectrolyte deposition and rinsing steps, which take up to several hours.

3. Plasmonic hydrogel sensors

Localized surface plasmon resonance (LSPR) is an optical phenomenon in noble metal nanostructures involving sharp spectral absorption and scattering that allow them to be used as sensors. A plasmon refers to the oscillation of the free electrons in a noble metal (Mayer and Hafner, 2011). When the surface plasmons are optically excited, light is coupled into propagating or standing surface modes (Rochon and Lévesque, 2006). When a surface plasmon occurs around a nanoparticle sized on the order of the wavelength of the light, the free electrons produce a collective oscillation, which is called LSPR. This enhances the electric fields near nanoparticles' surface, and this effect decreases with distance. The optical extinction of the nanoparticle corresponds to a maximum at the plasmon resonant frequency. The extinction peak depends on the nanoparticle type and its complex refractive index (Mayer and Hafner, 2011).

The LSPR can be utilized in hydrogels to sense external stimuli based on the changes in the position of the peak wavelength or intensity. Fig. 6a–d shows different configurations of plasmonic hydrogel sensors in thin films, array brush, core-shell colloids, and surface brush formats. Plasmonic nanoparticles have been incorporated in pH-responsive hydrogels. For example, gold nanoparticles were coated with pH-sensitive poly(methacrylic acid)-block-poly(*N*-isopropylacrylamide) (PMAA-*b*-PNIPAAm) (Nuopponen and Tenhu, 2007). In aqueous solutions, the nanoparticles aggregated as the pH was increased from 5 to 8. However, particle aggregation was irreversible. A blue shift in the LSPR was measured with decreasing pH or increasing temperature. Plasmonic crystal-based pH sensors were also reported (Mack et al., 2007). First, a metallic fold film (50 nm) was coated over a square array consisting of 350 nm deep cylindrical impressions with 480 nm diameter. A monomer mixture consisting of HEMA, EGDMA, AA, and aqueous surfactant (PEG hexadecyl ether) was photopolymerized over the substrate. As the pH in the environment was increased, the hydrogel volumetrically expanded and decreased the refractive index, shifting the LSPR peaks to shorter wavelengths. The sensor reversibly detected the changes within the pH range of 1.44–7.86, with a sensitivity of 0.1 pH units.

Lithographically fabricated gold nanocrescents, which were coated with a pH-sensitive pHEMA hydrogel matrix, have been reported (Jiang et al., 2009). The LSPR of these nanocrescents operated in the

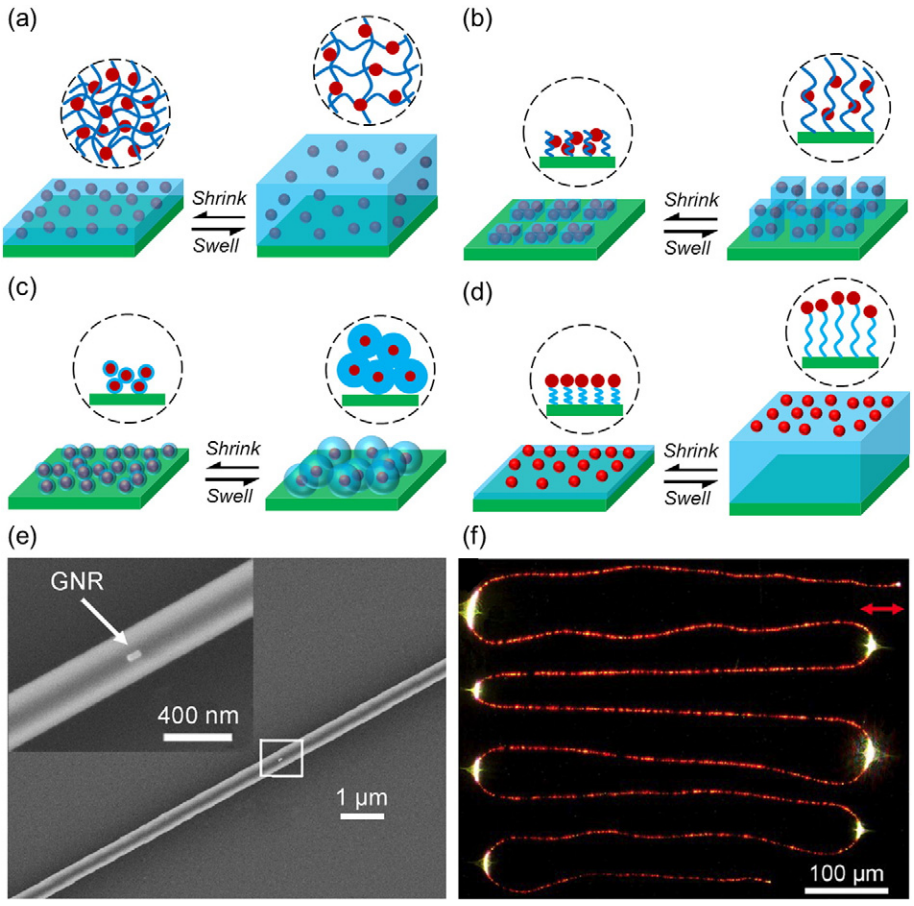

Fig. 6. Plasmonic hydrogel sensors. (a) Thin film hydrogel containing plasmonic nanoparticles, (b) microhydrogel array brush containing plasmonic particles, (c) 2D/3D assembly of core–shell colloids, (d) surface immobilized nanoparticles on the surface of a hydrogel brush, showing their microscale and their polymer architectures. (e) SEM image of a gold nanorod/pAAm nanofiber (Ø = 340 nm). The inset illustrates a magnified nanofiber where a gold nanorod was positioned. (f) Dark-field images of a gold nanorod embedded in a pAAm nanofiber (Ø = 440 nm, l = 4.1 mm) at parallel polarization. The white spots at the bended sections show scattered light. (e,f) Reprinted with permission from Wang et al. (2012), Copyright, American Chemical Society.

near-infrared region. As the pH was increased from pH 4.5 to 6.4, LSPR peaks shifted to shorter wavelengths, achieving an accuracy of 0.045 pH units. Plasmonic sensors based on polymer brushes were also synthesized (Tokareva et al., 2004). Gold nanoparticles attached to poly(2-vinylpyridine) (P2VP) polymer brushes over gold nanoislands allowed reversible monitoring of pH changes by transmission spectroscopy. When the pH was changed from 5.0 to 2.0, the polymer brushes swelled from 8.1 to 24.0 nm. This volumetric change shifted the absorption maximum of the transmission SPR spectrum of the supporting nanoislands by 50 nm. Furthermore, light-controlled switching was demonstrated for gold nanorods encapsulated in the thermoresponsive PNIPAAm shells (Rodríguez-Fernández et al., 2011). Gold nanorod cores were simultaneously used as fast optothermal manipulators (switchers) and sensitive optical reporters of the hydrogel state based on the analysis of the shifting behavior of the nanorod longitudinal plasmon.

Plasmonic hydrogel sensors were also used for measuring concanavalin A (Morokoshi et al., 2004). Gold nanoparticles were functionalized with disulfide-carrying polymer with pendent glucose residues (poly(2-methacryloyloxyethyl d-glucopyranoside)). The binding of concanavalin A to glucose was measured by LSPR sensing, showing a concentration-dependent response with a limit of detection of 1.9 nM. Another study reported the synthesis of DNA arrays using SPR hydrogel probes (Okumura et al., 2005). DNA arrays were constructed by a surface modification technique for detecting K-*ras* point mutations, which are associated with the development of malignancies such as lung and colon cancer. A homobifunctional alkane dithiol was adsorbed on the surface of a gold film and was modified with ethylene glycol moiety, which supressed non-specific adsorption during SPR analyses. Streptavidin was immobilized on the thiol modified surface, where biotinylated DNA ligands were attached to create DNA arrays. Finally, DNA probes conjugated with CA-containing AAm nanospheres were bound to the target DNA in a sandwich configuration. The use of nanospheres produced an SPR signal enhancement and allowed the discrimination of a K-*ras* point mutation in the SPR difference image. Furthermore, polymer particles were doped with dyes to amplify the SPR signal originating from antibody–antigen interactions (Komatsu et al., 2006). Such particles enhance the SPR signal by changing the imaginary part of the refractive index. The colorant improved the signal about 100 fold as compared to non-amplified SPR signal. Another study utilized dye-doped polymers and SPR allowed sensing Cu^{2+} ions (Ock et al., 2001). The sensor consisted of a poly(vinyl chloride-*co*-vinyl acetate-*co*-vinyl alcohol) copolymer film doped with squarylium dye and operated based on the changes in the refractive index upon interacting with Cu^{2+} ions, with a sensitivity of 1 pM.

Plasmonic particles were coupled with MIPs to measure the concentration of cholesterol (Tokareva et al., 2006). Gold nanoislands with a mean diameter of 14.5 nm were deposited over a glass substrate, where the interisland distance was 35 nm. These islands were spin coated over a 3 nm poly(glycidyl methacrylate) (PGMA) layer, which was used to graft carboxyl-terminated P2VP over the substrate. Subsequently, gold nanoparticles (Ø = 12 nm) and cholesterol were absorbed by the P2VP matrix and crosslinked by a quaternization reaction involving 1,4-diiodobutane to create the MIP layer. This MIP layer was used to sense cholesterol, where a 56 nm shift in the absorption maximum of the gold nanoislands was measured by T-SPR spectroscopy. MIPs were also utilized to detect domoic acid on a gold chip *via* SPR (Lotierzo et al., 2004). Domoic acid is a marine neurotoxin that causes amnesic shellfish poisoning (Lelong et al., 2012). A gold surface was functionalized with a self-assembled monolayer of 2-mercaptoethylamine, and 4,4′-azobis(cyanovaleric acid) was linked to the surface *via* carbodiimide chemistry. A 40 nm MIP film consisting of poly(2-(diethylamino) ethyl methacrylate) and EGDMA was attached to the functionalized surface. The resulting system enabled the use of a competitive binding assay to be performed with free domoic acid and its conjugate, while using horseradish peroxidase as a reactive label. The sensor allowed the measurement of domoic acid in buffer solutions through SPR readouts, achieving a detection limit of 5 ng/mL. Table 4 shows the plasmonic hydrogel sensors and their sensitivities.

Recently, newer platforms have emerged for utilizing SPR as the sensing probe. For example, polymer nanofibers consisting of aligned gold nanorods were utilized for sensing humidity (Fig. 6e) (Wang et al., 2012). A gold nanorod-doped pAAm nanofiber at parallel polarization showed red scattered light (Fig. 6f). The 540 nm thick nanofiber waveguides were illuminated at 785 nm from one end, and the intensity of the light output was measured from the other end. The scattering intensity of the waveguide decreased as the RH was increased. The sensor had a photon-to-plasmon conversion efficiency of 70% at its longitudinal resonance wavelength, and it allowed quantifying RH (10–70%) within 110 ms using 500 pW.

4. Reflection and refractive index modulation-based hydrogel sensors

Changes in the refractive index can be used as a measurement mechanism in hydrogel matrixes that can dynamically respond to a target analyte. For example, hydrogel microlenses were utilized as optical sensors due to changes in the refractive index or radius of curvature (Ehrick et al., 2007). The response due to swelling can be quantified by measuring the focusing power of the microlens (Fig. 7a, b). When a hydrogel lens interacts with a target analyte, the degree of de/focusing of the lens can be correlated with the concentration. The microdome patterned hydrogels were synthesized by UV or thermally initiated free-radical polymerization over a glass substrate. The hydrogel microdomes consisted of AAm copolymerized with calmodulin and phenothiazine derivatives. In the presence of the competing ligand chlorpromazine, calmodulin displaced phenothiazine, causing decrosslinking and gel swelling. This swelling changed the curvature of the microdome and its refractive index, subsequently defocusing the image. Microlenses were also constructed from hydrogel rings to control the curvature of a water–oil interface (Dong et al., 2006). These rings were created from PNIPAAm and functionalized with AA to create sensitivity for temperature and pH, respectively. The microlenses were produced by sandwiching a hydrogel ring between a glass surface and a hole, where the water was added, and oil was confined in this space. This produced a system with a water–oil interface at the center of the hydrogel ring. The curvature of the interface was modulated by volumetrically changing the hydrogel matrix through pH or temperature.

The synthesis of thermosensitive PNIPAAm-*co*-AA microgels on aminopropyltrimethoxysilane (APTMS) functionalized glass substrate has been reported (Serpe et al., 2004). Electrostatic interactions allowed amine groups on the substrate to bind to the AA functionalized microgels. Upon attachment to the substrate and drying, the microgels deformed isotropically. The microgel curvature was modulated by changing the temperature, pH and solvents. The resulting structures were used as dynamically tunable lenses through the modulation of the size, focal length, and the refractive index (Kim et al., 2004). Furthermore, these microlenses were tuned with laser light. A glass substrate was doped with gold nanoparticles (Ø = 16 nm), and a cationic polyelectrolyte PAH was deposited on this surface to render it positively charged (Kim et al., 2005b). PNIPAAm-*co*-AAc microgels were dropwise added to this system over the surface in a spatial manner. The resulting lens was excited with a frequency-doubled Nd:YAG laser ($\lambda = 532$ nm) at the plasmon modes on the gold nanoparticles. Based on the same principle, microlenses that display refractive index changes were designed for protein sensing (Kim et al., 2005a, 2006, 2007a,b). These microlenses consisted of binding- and displacement-induced formats. Biotin was conjugated to AA within the microlens, and the assay was tested in the presence of avidin or anti-biotin (antibody). Their presence increased the surface crosslinking of the microlens, which induced a

Table 4
Plasmonic sensors and their applications in medical diagnostics.

Stimulus	Recognition group	Dynamic range	Sensitivity	Ref.
pH	CA	3–12 units	12.5–19.5 nm/pH	Mishra and Gupta (2013), Singh and Gupta, (2012)
Glucose	Phenylboronic acid	<50 mM	50 μM	Mesch et al. (2015)
Melamine	Gold nanoparticles	1 μg/mL	1 μM	Manikas et al. (2014)
Concanavalin A	Molecular imprinting	1 μM	0.5° resonance angle shift/min	Kuriu et al. (2014)
Protein (FKBP12)	Carboxylated dextran	<10 nM	0.5 nM	Li et al. (2015a)
Trinitrotoluene	Molecular imprinting	83–250 μM	50 μM	Cennamo et al. (2013)
3-Pyridinecarboxamide	Molecular imprinting	0–10 mg/mL	1.483 nm/(mg/mL)	Verma and Gupta (2013)
Bisphenol A	Molecular imprinting	<0.5 mg/dL	0.05 mg/dL	(Taguchi et al., 2012)
4-Mercapto-benzoic acid	Matrix interaction	$10–10^4$ nM	65 pM	Ouyang et al. (2015)
2,2-Dipyridyl	Matrix interaction	$10–10^4$ nM	6.4 nM	Ouyang et al. (2015)
Water content in ethanol	Matrix interaction	<10 vol%	0.5 vol%	Mishra and Gupta (2014)

refractive index change. Using an inverted microscope, a single square projection was transited to double image.

A layer of functionalized microgels has been sandwiched between two gold films to produce an etalon. Upon interacting with an analyte, functionalized microgels produced volumetric changes, resulting in visual color changes and shifts in multipeak reflectance spectra. The positions of the peaks in the spectra primarily depended on the distance between the gold layers mediated by the microgel thickness. Reductant-sensitive PNIPAAm microgels crosslinked with *N*,*N*′-bis(acryloyl)cystamine have been synthesized and incorporated in an etalon (Li et al., 2015b). This device produced an optical response in the presence of dithiothreitol due to decrosslinking of the microgel matrix. The reflection peak of the etalon shifted ~45 nm as the concentration of dithiothreitol was increased from 0.19 to 1.50 mg/mL. Etalons were also used to sense ethanol (Huang and Serpe, 2015). As the concentration of ethanol was increased to 12 vol%, the reflectance peak shifted 60 nm to longer wavelengths. In another study, etalons were constructed from poly(*N*-isopropylacrylamide-*co*-*N*-(3-aminopropyl) methacrylamide hydrochloride) (PNIPAAm-*co*-APMAH) microparticles, which were functionalized to be sensitive to negatively charged single stranded DNA (ssDNA) (Islam and Serpe, 2014). In the presence of target DNA (80 μM, pH 7.2), the reflectance peak shifted 60 nm to shorter wavelengths. Etalons constructed from pyridine-functionalized PNIPAAm have been used for gas sensing (Zhang et al., 2015). As the CO_2 was introduced to the etalon, the reflectance peak shifted ~35 nm. However, the readouts of etalons are broadband, which may limit colorimetric measurements by eye. Nevertheless, as compared to the other hydrogel sensors, etalons are easier to fabricate.

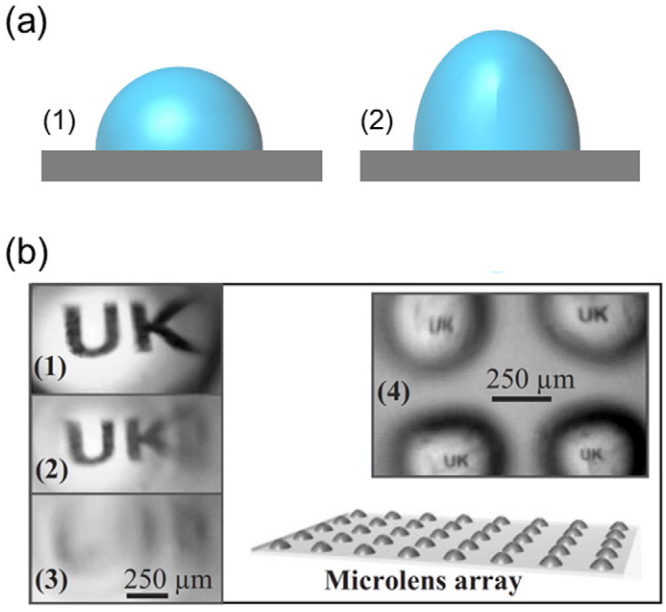

Fig. 7. Reflection and refractive index based hydrogel sensors. (a) A schematic of a tunable hydrogel microlens in (1) the initial state and (2) swollen in the presence of an analyte. (b) Image focused through a pAAm microlens in (1) the swollen state and (2, 3) defocused in a less swollen states. (4) The microlens array format. Reprinted with permission from Ehrick et al. (2007), Copyright, Wiley-VCH Verlag GmbH&Co. KGaA, Weinheim.

Analytes can also be sensed by a polymer-coated optical fiber tip. Optical fibers have several advantages such as remote sensing over long distances, small size and wave guiding as compared to other optical sensors. The change in refractive index and swelling can be read out by measuring the reflectance or by an interferometric setup. In one embodiment, a pH sensor was created by dip coating a fiber with Kraton, which was a styrene-ethylene, butylene-styrene, and a triblock copolymer (Shakhsher et al., 1994). In its non-swollen state, the polymer was opaque. However, when the pH was decreased from 8.0 to 6.5, the amine groups were protonated; hence, the polymer swelled and became transparent. The change in refractive index and clarity decreased the intensity of the reflected light by a factor of 2. To improve the sensitivity to the changes in refractive index, an interference method was used (Wei Chang et al., 2012). The fiber could be bitapered or a core offset could be introduced so that part of the core mode leaked into the cladding layer. Both core and cladding modes were reflected back from the coated fiber tip and were recombined in the fiber core. The optical path length difference between the two modes resulted in an interference pattern. The interference was measured by using a tunable laser as a light source and recording the output intensity as a function of its wavelength. Refractive index change was proportional to the wavelength shift of the interference. In another study, a bitapered optical fiber was coated with polyvinyl alcohol (PVA)/PAA hydrogel. A sensitivity of 1.58 nm/pH was achieved in the range of 2.48–6.47 (Wong et al., 2014).

Swellable polymer microspheres dispersed in hydrogels can also be used as sensors. Such dispersions are optically opaque because of the mismatch of the refractive index of the spheres and the hydrogel, causing light scattering. Upon introduction of an analyte, the polymer particles change refractive index, scattering, and turbidity. The polymer microsphere method has advantages over surface immobilized polymers since the microspheres are free to swell in all directions in the hydrogel matrix, eliminating the problems of deformation, cracking and detachment of the polymer layer. Furthermore, light transmission can be measured at any wavelength with standard equipment such as a UV/Vis/NIR spectrometer. For example, a pH sensor has been made of a dispersion of aminated poly(vinylbenzyl chloride) microspheres (Ø = 1 μm) suspended in a pHEMA matrix (Rooney and Seitz, 1999). Turbidity was measured when pH was changed from pH 4.0 to 10.0. In another study, pH-sensitive polymer particles were synthesized from NIPAAm copolymerized with a pH sensitive functional comonomer and embedded in a PVA matrix (Lavine et al., 2012).

5. Tests in biological and clinical samples

Photonic hydrogel sensors have been tested in blood and urine samples to analyze the interference from other analyte species. Holographic sensors containing phenylboronic acid (12 mol%), and trimethylammonium chloride (12 mol%) have been used to measure the concentration of glucose (3–33 mmol L^{-1}) in seven human blood plasma samples (Worsley et al., 2007). Trimethylammonium chloride increased the sensitivity of phenylboronic acid to glucose over other saccharides possessing *cis*-1,2- or -1,3-diols (Horgan et al., 2006). The measurements were calibrated with an electrochemical analyzer (2300 STAT Plus). As the concentration of glucose was increased from 3.8 mmol L^{-1} to 30.9 mmol L^{-1}, the Bragg peak shifted from 640 to 571 nm. The reproducibility and repeatability of the holographic sensors were 1.9–5.4 and 1.1–4.8, respectively. However, this approach required buffering the sample using sodium phosphate to keep pH constant at 7.4. Holographic sensors were also tested with urine samples of diabetic patients (Yetisen et al., 2014d). These sensors containing 3-APB (20 mol%) responded to glucose (2–10 mM) by changing their color from green to red. In clinical tests, the sensors were able to measure glucose up to 400 mmol L^{-1} within 3 min with a detection limit of 90 μM. A significant challenge with the readouts of phenylboronic acid is that *cis*-diol binding with glucose requires ~1–2 h to reach saturation. To shorten the response time, an algorithm was developed to correlate the concentration of glucose with the binding rate, and the readouts were achieved in 3 min. However, the interaction of 3-APB with glucose was pH dependent; hence, the measurements were conducted under fixed pH conditions.

An ammonia-sensitive CCAs has been tested with human blood serum (Kimble et al., 2006). This CCA included covalently attached 3-aminophenol to the pHEA matrix, which formed crosslinks through Berthelot mechanism. Ammonia present in a solution reacted with hypochlorite to form a monochloramine, which in turn reacted with pendant 3-aminophenols to create a crosslink in the hydrogel matrix. pK_a values of 3-aminophenol are 4.37 and 9.81 for the amine and hydroxy groups, respectively. The crosslink formation in the hydrogel shifted the diffracted light to shorter wavelengths in proportion to the amount of ammonia present in the solution. The sensors tested in diluted human blood serum in borate buffer (pH 9, 50 mmol L^{-1}) showed Bragg peak shifts of 2, 4, 7, and 13 nm in the presence of 30, 75, 150, and 300 μmol L^{-1} ammonia within 1 h, respectively. The detection limit of this sensor was 50 μmol L^{-1} (Kimble et al., 2006). A limitation of this sensor was that the samples required highly basic buffers to function. Furthermore, CCAs functionalized with 8HQ have been used to measure Ni^{2+} ions in human plasma at neutral pH (Baca et al., 2008). pAAm matrix containing CCAs was first hydrolyzed at 24 °C for 2 h. 1-ethyl-3-(3-dimethylaminopropyl)carbodiimide (EDC)-initiated condensation reaction was used to covalently link 5-amino-8HQ to the pAAm matrix. When human plasma (10 mL) was added to $NiCl_2$ (0.75 mmol L^{-1}, 20 mL) in HEPES (pH 7.4, 50 mmol L^{-1}) buffer and NaCl (150 mmol L^{-1}), the Bragg peak of the sensor shifted 12.4 nm to shorter wavelengths. This Ni^{2+} sensor had a sensitivity of 60 μmol L^{-1} (Baca et al., 2008). However, blood plasma has a complex composition containing proteins and ions that contract the pAAm matrix due to a decrease in Donnan osmotic pressure.

Porous silicon sensors were tested in opiate spiked human urine samples (n = 50) (Bonanno et al., 2010). Porous silicon was functionalized with an opiate-analogue (MG3). This was achieved *via* carbodiimide chemistry by linking MG3 to lysine groups present on a bovine serum albumin blocked surface. In oxycodone-free urine samples, monoclonal mouse antimorphine antibody (α-M Ab) bound to the opiate-analogue attached to silicon pore surface, which resulted in a 6 nm Bragg peak shift to longer wavelengths. Free opiates in urine competed for binding sites on the α-M Ab, and this resulted in a corresponding decrease in the wavelength shift. Limitations of porous silicon sensors include variation in the pore diameters, and readouts below 10 nm that are not possible to identify with eye.

6. Future directions

Many bottom-up fabrication methods including layer-by-layer assembly, and spin- and dip-coating require the deposition of nanoparticle and polymer bilayers with accuracy. In these approaches, the accuracy of the assembly depends on the sequential coating steps, which are time consuming. Faster deposition schemes might be achieved through automation and 3D printing (Xing et al., 2015). For example, robotic coaters have been utilized in the spray layer-by-layer assembly of polyelectrolytes and TiO_2 and SiO_2 multilayers (Nogueira et al., 2011). Such methods can achieve assembly faster than the immersion layer-by-layer deposition. Increasing the control of deposition parameters such as temperature, spinning and withdrawal times, the quantity and the concentration of solutions through robotics will allow creating uniform optical properties in centimeter-sized substrates. The broader use of ink-jet type material deposition systems will enable precise localization of the analyte sensitive species and the production of patterned gratings. Such devices may have the ability to convey a message at the moment of analyte detection. Furthermore, these approaches can include novel materials such as graphene, carbon nanotubes, quantum dots, magnetic nanoparticles, silk, nanofibers, nanocrystals, latex particles, and negative refractive index structures (Butt et al., 2015; Deng et al., 2014; Kong et al., 2014, 2015).

In visually read optical sensors, a significant limitation is the visibility of the photonic structures from wide angles. The semi-quantitative readout of photonic hydrogel sensors by eye is challenging. For example, in Bragg reflectors, the color of the diffracted light might depend on the position of the observer. Furthermore, as the hydrogel swells and shrinks, the angle of the diffracted light from the normal to the surface plane changes; this is an inherent property of Bragg reflectors. A significant contribution to the area would be the development of omnidirectional gratings that can be fabricated with high refractive-index contrast constituent layers. The incorporation of diffusers, lenses, reflectors, or other optical devices in photonic gratings will improve the angle of view (Zhao et al., 2015b). Some of these fabrication approaches may be inspired from structural color designs in nature (Oh et al., 2014). However, such additional features may decrease the intensity of the diffracted light in any given direction. Hence, the optimization of Bragg stack layers or the concentration of plasmonic nanomaterials in the hydrogel matrix will increase the diffraction efficiency of photonic sensors. Additionally, the development of algorithms that can estimate the position of the Bragg peak as the hydrogel matrix swells or shrinks will be a valuable contribution. Another potential area of development is tuning the sensors to operate in the entire visible spectrum; currently, only a few sensors have utilized broad colorimetric regions.

Photonic hydrogel sensors have high sensitivity ranging from pM to mM. However, a limiting factor for realizing the full potential of photonic hydrogel sensors is selectivity. Ionic strength, pH and temperature significantly affect the performance of photonic hydrogel sensors. The development of environmental-factor independent affinity ligands to control the selectivity of targeting by antibodies and bioactive macromolecules such as nucleic acids and whole cells will be important contributions to the field. Photonic hydrogels may be multiplexed to improve the dynamic range and obtain readouts from different sensors. Moreover, the integration of photonic hydrogel sensors with PDMS or paper-based microfluidics may allow multiplexing (Volpatti and Yetisen, 2014; Yetisen, 2015g; Yetisen and Volpatti, 2014). Such assays enable the use of low-volumes of fluids to carry out sample preparation for high-throughput analyses (Choi and Cunningham, 2007; Kim et al., 2014). Additionally, testing the effects of batch-to-batch variability, oxidation, material decay, and long-term storage can be significant contributions in creating robust hydrogel sensors. Fabrication techniques that allow constructing sensors from microporous hydrogels are

required to increase diffusion rates. For example, fabrication of photonic structures utilizing zeolite nanoparticles could be a feasible method to increase the response time of the sensors. Additionally, while the hydrogel sensors that do not selectively bind to analytes had fast response times, the sensors with ligands take inherently longer times to bind to target analytes and reach equilibrium. This remains a significant issue as compared to electrochemical sensing. Investigations in binding kinetics of chelating agents and ligands, and reversibility will enable the development of photonic hydrogel sensors with improved control over selectivity in addition to rapid response time. Studies in shrinking/swelling dynamics, non-specific interactions with hydrogel matrix, surface energy and charge, hydrophilicity/phobicity, surface roughness, and polymer porosity will allow the rational design of sensors. Furthermore, the models that can simulate the properties of material during swelling and shrinking cycles, change in effective refractive index, plasmonic effects, diffraction and absorption spectra of the grating or the nanoparticles/dopants will contribute to the theoretical understanding of photonic hydrogel sensors.

Readout technologies of photonic hydrogel sensors should also evolve. Smartphone technologies have recently emerged as a platform to quantify the sensor readouts while offering connectivity options (Yetisen et al., 2014b,c). This platform will also enable the real time reporting of the results of IVD testing. For example, readouts of photonic hydrogel sensors with tablet computers, smartphones/watches, or other wearable technologies can improve the existing user interface. The embedded light sources in these mobile devices may be utilized to standardize the illumination of the sensors. Such platforms also provide data processing capability to mitigate the interference from background noise of the sample or ambient light. While these readout technologies are required for quantitative analyses, there is also a significant market need for equipment free semi-quantitative diagnostics, where photonic hydrogel sensors may offer solutions through their colorimetric readouts. Such devices may also include user-friendly foolproof text or image reporting capabilities. Additionally, photonic hydrogels are not limited to IVD, but also offer possibilities in implantable chips (Choi et al., 2013) and contact lens sensors (Farandos et al., 2015), where long-term operation, biocompatibility are required for continuous quantification of analytes *in vivo*.

7. Conclusions

Many top-down and bottom-up approaches including laser writing, self-assembly and layer-by-layer deposition have been demonstrated to create Bragg diffraction gratings, microlenses, etalons and plasmonic structures in hydrogels. These hydrogels have been functionalized to be sensitive to a wide range of analytes by creating covalently-bound pendant recognition groups or molecularly imprinted sites. Utilizing the nanoscale structures as transducers, functionalized hydrogel matrixes have been utilized to quantitatively report on the concentrations of target analytes. When these sensors output narrow-band light over broad wavelength ranges in the visible spectrum, the readouts were visible to the eye for semi-quantitative analyses. Fully-quantitative readouts were obtained using spectrophotometers.

The majority of photonic hydrogel sensors have been created by self-assembly. However, most approaches require lengthy syntheses to create Bragg gratings. For example, forming monodisperse, highly-charged PS particles through emulsion polymerization require lengthy dialysis times. The creation of high-quality CCAs with large areas still require hours to days to complete. Furthermore, CCAs suffer from defects since the properties of highly charged particles cannot be controlled precisely. Other self-assembly approaches including layer-by-layer deposition and spin coating suffer from instability and time-consuming fabrication. For instance, formation of organic–inorganic Bragg stacks is limited due to the instability of the polymer in the presence of acidic inorganic sol, which distorts the morphological integrity of the sublayer.

Inclusion of charged functional groups during self-assembly and polymerization disrupts the lattice spacing in CCAs, block copolymers, and Bragg stacks. Hence, the functionalization of the polymer matrix often needs to be performed post-hydrogel formation. This results in nonuniform distributions of functional moieties throughout the hydrogel matrix. In inverse opals, the diffraction efficiency is relatively higher as compared to the CCAs, but they also suffer from lattice disruption. Block copolymers such as PS-b-PAA and PS-b-P2VP are fundamentally limited to pH and unspecific solvent sensing. Additionally, self-assembly approaches lack flexibility in controlling the dimensions of the sensors. For instance, sedimentation and centrifugation do not have precise control over sample thickness. Other approaches involving layer-by-layer deposition is limited to thin films. Although many applications have been demonstrated utilizing self-assembled sensors, few of them utilized the entire visible spectrum to report on the analyte concentrations. Most applications have wavelength shifts smaller than 10 nm, not visible to the eye. In particular, due to high crosslinker concentration, MIPs suffer from small wavelength shifts. Hence, tuning range of Bragg peak shifts requires improvement in polymer synthesis, potentially involving increased porosity and hydrophilicity. Broad wavelength shifts and the entire visible spectrum need to be utilized for practical colorimetric sensing applications.

In contrast to self-assembly, top-down techniques such as holographic patterning offers reproducibility. In fabricating holographic sensors, charged functional groups can be incorporated during polymerization prior to Bragg grating formation. The lattice spacing of holographic sensors can be easily tuned using different wavelengths of laser light. A challenge associated with holographic sensing is that achieving high diffraction efficiency requires multiple processing steps in silver halide chemistry. While high-energy laser patterning of holographic sensors can be completed in a few steps, this approach suffers from low diffraction efficiency (<10%). Photopolymerization-induced formation of Bragg gratings is a practical approach to create Bragg gratings; however, the migration of short polymer chains during high-intensity recording results in low diffraction efficiency. Nevertheless, holographic patterning offers fabrication flexibility that cannot be achieved with bottom-up approaches.

Hydrogel microlenses provide a simpler fabrication approach as compared to the Bragg grating-based hydrogel sensors. This approach does not require complicated fabrication approaches, and the output of the assay is the changes in the refractive index or the focus of the lens. However, this approach requires significant changes in the refractive index to create a resolvable shift in the spectrophotometer. This approach also falls short as a mobile rapid diagnostic assay since the measurements require an external photodetector. Fiber optic sensors incorporate hydrogels and a quantitative spectrometry within the same device; and since the hydrogel matrix is in direct contact with the fiber, the readouts are more accurate compared to other sensing platforms. Furthermore, plasmonics is a flexible approach to create photonic hydrogel sensors, but the ability to tune the colors of plasmonic assays and the capability to obtain color changes in the entire visible spectrum is yet to be demonstrated, limiting the use of this assay to yes/no readouts or spectrophotometric analysis.

Existing IVD technologies are primarily based on molecular dyes, electrochemistry, and gold nanoparticle-based lateral-flow assays. These assays cannot colorimetrically display quantitative results, and they have limited use in repeat analyses. Additionally, the incorporation of many recognition agents using a single platform is challenging for traditional assays. This market gap represents an opportunity to develop quantitative photonic hydrogel sensors that can operate in the entire visible spectrum. Photonic hydrogels should offer improvement in sensitivity, selectivity, response time, and user interface to create a competitive advantage and unique selling point. Potential applications may focus on reusable, wearable, and equipment-free colorimetric IVD devices. Another niche area is localized sensing and mapping the concentrations of analytes throughout a sample. The value of photonic

hydrogel sensors can only be realized if they offer a strategic advance over existing products, are compatible with existing manufacturing lines, and show efficacy at point-of-care settings.

Author contributions

A.K.Y. and S.H.Y. designed the review. A.K.Y. wrote the manuscript. L.R.V. contributed to Crystalline Colloidal Array Sensors. M.H. contributed to Reflection and Refractive Index Modulation-Based Hydrogel Sensors. S.H.Y., L.R.V., I.P., I.N., K.S.K., H.K., S.K.H., S.J.J.K, and A.K. edited the manuscript.

Acknowledgments

This work was supported in part by the National Institutes of Health (P41EB015903), National Science Foundation (ECCS-1505569, CBET-264356), Department of Defence (FA9550-11-1-0331), the Bio & Medical Technology Development Program (No. 2012M3A9C6049791) and IT Consilience Creative Program (No. NIPA-2014-H0201-14-1001). M.H. was supported by Marie Curie International Outgoing Fellowship (No. 627274). We thank Jeff Blyth, Sanford Asher, and Geoffrey A. Ozin for their discussions.

References

Aguirre, C.I., Reguera, E., Stein, A., 2010. Tunable colors in opals and inverse opal photonic crystals. Adv. Funct. Mater. 20, 2565–2578.
Akram, M.S., Daly, R., Vasconcellos, F.C., Yetisen, A.K., Hutchings, I., Hall, E.A.H., 2015. Applications of Paper-Based Diagnostics. In: Castillo-León, J., Svendsen, W.E. (Eds.), Lab-on-a-Chip Devices and Micro-Total Analysis Systems. Springer International Publishing, pp. 161–195.
Alexeev, V.L., Sharma, A.C., Goponenko, A.V., Das, S., Lednev, I.K., Wilcox, C.S., et al., 2003. High ionic strength glucose-sensing photonic crystal. Anal. Chem. 75, 2316–2323.
Anzai, J.-I., Kobayashi, Y., Nakamura, N., Nishimura, M., Hoshi, T., 1999. Layer-by-layer construction of multilayer thin films composed of avidin and biotin-labeled poly(amine)s. Langmuir 15, 221–226.
Araki, K., Wagner, M.J., Wrighton, M.S., 1996. Layer-by-layer growth of electrostatically assembled multilayer porphyrin films. Langmuir 12, 5393–5398.
Archer, F., 1851. On the use of collodion in photography. Chemist 2, 257–258.
Arsenault, A., Fleischhaker, F., von Freymann, G., Kitaev, V., Miguez, H., Mihi, A., et al., 2006. Perfecting imperfection—designer defects in colloidal photonic crystals. Adv. Mater. 18, 2779–2785.
Arunbabu, D., Sannigrahi, A., Jana, T., 2011. Photonic crystal hydrogel material for the sensing of toxic mercury ions (Hg^{2+}) in water. Soft Matter 7, 2592–2599.
Asher, S.A., 1986. Crystalline Colloidal Narrow Band Radiation Filter. US Patent 4627689 A.
Asher, S.A., Holtz, J.H., 1998. Novel Polymerized Crystalline Colloidal Array Sensors. WO Patent application 019787A1.
Asher, S.A., Holtz, J., Liu, L., Wu, Z., 1994. Self-assembly motif for creating submicron periodic materials. Polymerized crystalline colloidal arrays. J. Am. Chem. Soc. 116, 4997–4998.
Asher, S.A., Peteu, S.F., Reese, C.E., Lin, M., Finegold, D., 2002. Polymerized crystalline colloidal array chemical-sensing materials for detection of lead in body fluids. Anal. Bioanal. Chem. 373, 632–638.
Asher, S.A., Alexeev, V.L., Goponenko, A.V., Sharma, A.C., Lednev, I.K., Wilcox, C.S., et al., 2003. Photonic crystal carbohydrate sensors: low ionic strength sugar sensing. J. Am. Chem. Soc. 125, 3322–3329.
Ayyub, O.B., Ibrahim, M.B., Briber, R.M., Kofinas, P., 2013. Self-assembled block copolymer photonic crystal for selective fructose detection. Biosens. Bioelectron. 46, 124–129.
Baca, J.T., Finegold, D.N., Asher, S.A., 2008. Progress in developing polymerized crystalline colloidal array sensors for point-of-care detection of myocardial ischemia. Analyst 133, 385–390.
Bachmann, C., 2003. Outcome and survival of 88 patients with urea cycle disorders: a retrospective evaluation. Eur. J. Pediatr. 162, 410–416.
Banwell, E.F., Abelardo, E.S., Adams, D.J., Birchall, M.A., Corrigan, A., Donald, A.M., et al., 2009. Rational design and application of responsive α-helical peptide hydrogels. Nat. Mater. 8, 596–600.
Barry, R.A., Wiltzius, P., 2006. Humidity-sensing inverse opal hydrogels. Langmuir 22, 1369–1374.
Bates, F.S., Fredrickson, G.H., 1990. Block copolymer thermodynamics: theory and experiment. Annu. Rev. Phys. Chem. 41, 525–557.
Bates, F.S., Fredrickson, G.H., 2008. Block copolymers—designer soft materials. Phys. Today 52, 32–38.
Bhatta, D., Christie, G., Madrigal-Gonzalez, B., Blyth, J., Lowe, C.R., 2007. Holographic sensors for the detection of bacterial spores. Biosens. Bioelectron. 23, 520–527.
Bhatta, D., Christie, G., Blyth, J., Lowe, C.R., 2008. Development of a holographic sensor for the detection of calcium dipicolinate—a sensitive biomarker for bacterial spores. Sensors Actuators B 134, 356–359.
Blanquart-Evrard, L.-D., 1847. Procédés employés pour obtenir les épreuves de photographie sur papier. C. Chevalier.
Blyth, J., Millington, R.B., Mayes, A.G., Frears, E.R., Lowe, C.R., 1996. Holographic sensor for water in solvents. Anal. Chem. 68, 1089–1094.
Blyth, J., Millington, R.B., Mayes, A.G., Lowe, C.R., 1999. A diffusion method for making silver bromide based holographic recording material. Imaging Sci. J. 47, 87–92.
Bockstaller, M., Kolb, R., Thomas, E.L., 2001. Metallodielectric photonic crystals based on diblock copolymers. Adv. Mater. 13, 1783–1786.
Bockstaller, M.R., Mickiewicz, R.A., Thomas, E.L., 2005. Block copolymer nanocomposites: perspectives for tailored functional materials. Adv. Mater. 17, 1331–1349.
Bonanno, L.M., DeLouise, L.A., 2007. Whole blood optical biosensor. Biosens. Bioelectron. 23, 444–448.
Bonanno, L.M., DeLouise, L.A., 2010. Integration of a chemical-responsive hydrogel into a porous silicon photonic sensor for visual colorimetric readout. Adv. Funct. Mater. 20, 573–578.
Bonanno, L.M., Kwong, T.C., DeLouise, L.A., 2010. Label-free porous silicon immunosensor for broad detection of opiates in a blind clinical study and results comparison to commercial analytical chemistry techniques. Anal. Chem. 82, 9711–9718.
Bonifacio, L.D., Lotsch, B.V., Puzzo, D.P., Scotognella, F., Ozin, G.A., 2009. Stacking the nanochemistry deck: structural and compositional diversity in one-dimensional photonic crystals. Adv. Mater. 21, 1641–1646.
Boulmedais, F., Ball, V., Schwinte, P., Frisch, B., Schaaf, P., Voegel, J.-C., 2003. Buildup of exponentially growing multilayer polypeptide films with internal secondary structure. Langmuir 19, 440–445.
Brust, M., Walker, M., Bethell, D., Schiffrin, D.J., Whyman, R., 1994. Synthesis of thiol-derivatised gold nanoparticles in a two-phase liquid–liquid system. J. Chem. Soc. Chem. Commun. 801–802.
Brynda, E., Houska, M., 1996. Multiple alternating molecular layers of albumin and heparin on solid surfaces. J. Colloid Interface Sci. 183, 18–25.
Bucknall, D.G., Anderson, H.L., 2003. Polymers get organized. Science 302, 1904–1905.
Buenger, D., Topuz, F., Groll, J., 2012. Hydrogels in sensing applications. Prog. Polym. Sci. 37, 1678–1719.
Burgess, I.B., Loncar, M., Aizenberg, J., 2013. Structural colour in colourimetric sensors and indicators. J. Mater. Chem. C 1, 6075–6086.
Butt, H., Yetisen, A.K., Ahmed, R., Yun, S.H., Dai, Q., 2015. Carbon nanotube biconvex microcavities. Appl. Phys. Lett. 106, 121108.
Cai, Z., Liu, Y.J., Lu, X., Teng, J., 2013. In situ "doping" inverse silica opals with size-controllable gold nanoparticles for refractive index sensing. J. Phys. Chem. C 117, 9440–9445.
Cai, Z., Zhang, J.-T., Xue, F., Hong, Z., Punihaole, D., Asher, S.A., 2014. 2D photonic crystal protein hydrogel coulometer for sensing serum albumin ligand binding. Anal. Chem. 86, 4840–4847.
Cai, Z., Smith, N.L., Zhang, J.-T., Asher, S.A., 2015. Two-dimensional photonic crystal chemical and biomolecular sensors. Anal. Chem. 87, 5013–5025.
Carlson, R.J., Asher, S.A., 1984. Characterization of optical diffraction and crystal structure in monodisperse polystyrene colloids. Appl. Spectrosc. 38, 297–304.
Cate, D.M., Adkins, J.A., Mettakoonpitak, J., Henry, C.S., 2015. Recent developments in paper-based microfluidic devices. Anal. Chem. 87, 19–41.
Cennamo, N., D'Agostino, G., Galatus, R., Bibbo, L., Pesavento, M., Zeni, L., 2013. Sensors based on surface plasmon resonance in a plastic optical fiber for the detection of trinitrotoluene. Sensors Actuators B 188, 221–226.
Chen, C., Zhu, Y., Bao, H., Shen, J., Jiang, H., Peng, L., et al., 2011. Ethanol-assisted multi-sensitive poly (vinyl alcohol) photonic crystal sensor. Chem. Commun. (Camb. U. K.) 47, 5530–5532.
Chiappelli, M.C., Hayward, R.C., 2012. Photonic multilayer sensors from photo-crosslinkable polymer films. Adv. Mater. 24, 6100–6104.
Chin, C.D., Linder, V., Sia, S.K., 2012. Commercialization of microfluidic point-of-care diagnostic devices. Lab Chip 12, 2118–2134.
Chiu, J.J., Kim, B.J., Kramer, E.J., Pine, D.J., 2005. Control of nanoparticle location in block copolymers. J. Am. Chem. Soc. 127, 5036–5037.
Chiu, J.J., Kim, B.J., Yi, G.-R., Bang, J., Kramer, E.J., Pine, D.J., 2007. Distribution of nanoparticles in lamellar domains of block copolymers. Macromolecules 40, 3361–3365.
Choi, C.J., Cunningham, B.T., 2007. A 96-well microplate incorporating a replica molded microfluidic network integrated with photonic crystal biosensors for high throughput kinetic biomolecular interaction analysis. Lab Chip 7, 550–556.
Choi, M., Choi, J.W., Kim, S., Nizamoglu, S., Hahn, S.K., Yun, S.H., 2013. Light-guiding hydrogels for cell-based sensing and optogenetic synthesis in vivo. Nat. Photonics 7, 987–994.
Cooper, T.M., Campbell, A.L., Crane, R.L., 1995. Formation of polypeptide-dye multilayers by electrostatic self-assembly technique. Langmuir 11, 2713–2718.
Couturier, J.P., Sütterlin, M., Laschewsky, A., Hettrich, C., Wischerhoff, E., 2015. Responsive inverse opal hydrogels for the sensing of macromolecules. Angew. Chem. Int. Ed. 54, 6641–6644.
Cui, J., Zhu, W., Gao, N., Li, J., Yang, H., Jiang, Y., et al., 2014. Inverse opal spheres based on polyionic liquids as functional microspheres with tunable optical properties and molecular recognition capabilities. Angew. Chem. Int. Ed. 53, 3844–3848.
Danaei, G., Finucane, M.M., Lu, Y., Singh, G.M., Cowan, M.J., Paciorek, C.J., et al., 2011. National, regional, and global trends in fasting plasma glucose and diabetes prevalence since 1980: systematic analysis of health examination surveys and epidemiological studies with 370 country-years and 2.7 million participants. Lancet 378, 31–40.
Decher, G., 1997. Fuzzy nanoassemblies: toward layered polymeric multicomposites. Science 277, 1232–1237.
Decher, G., Hong, J., 1991. Buildup of ultrathin multilayer films by a self-assembly process: II. Consecutive adsorption of anionic and cationic bipolar amphiphiles and polyelectrolytes on charged surfaces. Ber. Bunsenges. Phys. Chem. 95, 1430–1434.

Decher, G., Hong, J., Schmitt, J., 1992. Buildup of ultrathin multilayer films by a self-assembly process: III. Consecutively alternating adsorption of anionic and cationic polyelectrolytes on charged surfaces. Thin Solid Films 210, 831–835.
DeLouise, L.A., Fauchet, P.M., Miller, B.L., Pentland, A.A., 2005. Hydrogel-supported optical-microcavity sensors. Adv. Mater. 17, 2199–2203.
Deng, S., Yetisen, A.K., Jiang, K., Butt, H., 2014. Computational modelling of a graphene Fresnel lens on different substrates. RSC Adv. 4, 30050–30058.
Denisyuk, Y.N., 1962. On the reflection of optical properties of an object in a wave field of light scattered by it. Dokl. Akad. Nauk SSSR 144, 1275.
Diabetes Atlas, 2013. 6 edn. International Diabetes Federation. Brussels, Belgium.
Diao, Y.Y., Liu, X.Y., Toh, G.W., Shi, L., Zi, J., 2013. Multiple structural coloring of silk-fibroin photonic crystals and humidity-responsive color sensing. Adv. Funct. Mater. 23, 5373–5380.
Domschke, A., March, W.F., Kabilan, S., Lowe, C., 2006. Initial clinical testing of a holographic non-invasive contact lens glucose sensor. Diabetes Technol. Ther. 8, 89–93.
Dong, L., Agarwal, A.K., Beebe, D.J., Jiang, H., 2006. Adaptive liquid microlenses activated by stimuli-responsive hydrogels. Nature 442, 551–554.
Dziri, L., Boussaad, S., Tao, N., Leblanc, R.M., 1998. Acetylcholinesterase complexation with acetylthiocholine or organophosphate at the air/aqueous interface: AFM and UV–vis studies. Langmuir 14, 4853–4859.
Edrington, A.C., Urbas, A.M., DeRege, P., Chen, C.X., Swager, T.M., Hadjichristidis, N., et al., 2001. Polymer-based photonic crystals. Adv. Mater. 13, 421–425.
Egen, M., Voss, R., Griesebock, B., Zentel, R., Romanov, S., Torres, C.S., 2003. Heterostructures of polymer photonic crystal films. Chem. Mater. 15, 3786–3792.
Ehrbar, M., Schoenmakers, R., Christen, E.H., Fussenegger, M., Weber, W., 2008. Drug-sensing hydrogels for the inducible release of biopharmaceuticals. Nat. Mater. 7, 800–804.
Ehrick, J.D., Deo, S.K., Browning, T.W., Bachas, L.G., Madou, M.J., Daunert, S., 2005. Genetically engineered protein in hydrogels tailors stimuli-responsive characteristics. Nat. Mater. 4, 298–302.
Ehrick, J.D., Stokes, S., Bachas-Daunert, S., Moschou, E.A., Deo, S.K., Bachas, L.G., et al., 2007. Chemically tunable lensing of stimuli-responsive hydrogel microdomes. Adv. Mater. 19, 4024–4027.
Farandos, N.M., Yetisen, A.K., Monteiro, M.J., Lowe, C.R., Yun, S.H., 2015. Contact lens sensors in ocular diagnostics. Adv. Healthc. Mater. 4, 792–810.
Ferrand, P., Egen, M., Zentel, R., Seekamp, J., Romanov, S., Torres, C.S., 2003. Structuring of self-assembled three-dimensional photonic crystals by direct electron-beam lithography. Appl. Phys. Lett. 83, 5289–5291.
Fink, Y., Urbas, A.M., Bawendi, M.G., Joannopoulos, J.D., Thomas, E.L., 1999. Block copolymers as photonic bandgap materials. J. Lightwave Technol. 17, 1963–1969.
Fleischhaker, F., Arsenault, A.C., Kitaev, V., Peiris, F.C., von Freymann, G., Manners, I., et al., 2005a. Photochemically and thermally tunable planar defects in colloidal photonic crystals. J. Am. Chem. Soc. 127, 9318–9319.
Fleischhaker, F., Arsenault, A.C., Wang, Z., Kitaev, V., Peiris, F.C., von Freymann, G., et al., 2005b. Redox-tunable defects in colloidal photonic crystals. Adv. Mater. 17, 2455–2458.
Fleischhaker, F., Arsenault, A.C., Peiris, F.C., Kitaev, V., Manners, I., Zentel, R., et al., 2006. DNA designer defects in photonic crystals: optically monitored biochemistry. Adv. Mater. 18, 2387–2391.
Folke, M., Cernerud, L., Ekström, M., Hök, B., 2003. Critical review of non-invasive respiratory monitoring in medical care. Med. Biol. Eng. Comput. 41, 377–383.
Fredrickson, G.H., Bates, F.S., 1996. Dynamics of block copolymers: theory and experiment. Annu. Rev. Mater. Sci. 26, 501–550.
Fuchs, Y., Soppera, O., Mayes, A.G., Haupt, K., 2013. Holographic molecularly imprinted polymers for label-free chemical sensing. Adv. Mater. 25, 566–570.
Fuchs, Y., Kunath, S., Soppera, O., Haupt, K., Mayes, A.G., 2014. Molecularly imprinted silver-halide reflection holograms for label-free opto-chemical sensing. Adv. Funct. Mater. 24, 688–694.
Fudouzi, H., 2011. Tunable structural color in organisms and photonic materials for design of bioinspired materials. Sci. Technol. Adv. Mater. 12, 064704.
Furumi, S., Fudouzi, H., Sawada, T., 2010. Self-organized colloidal crystals for photonics and laser applications. Laser Photonics Rev. 4, 205–220.
Gabor, D., 1948. A new microscopic principle. Nature 161, 777–778.
Gabor, D., 1949. Microscopy by reconstructed wave-fronts. Proc. R. Soc. A 197, 454–487.
Ge, J., Yin, Y., 2011. Responsive photonic crystals. Angew. Chem. Int. Ed. 50, 1492–1522.
Gerlach, G., Arndt, K.-F., 2009. Hydrogel Sensors and Actuators: Engineering and Technology. Springer Science & Business Media, Heidelberg.
Gonzalez, B.M., Christie, G., Davidson, C.A.B., Blyth, J., Lowe, C.R., 2005. Divalent metal ion-sensitive holographic sensors. Anal. Chim. Acta 528, 219–228.
Grand View Research, 2014. In-Vitro Diagnostics (IVD) Market Analysis and Segment Forecasts To 2020.
Griffete, N., Frederich, H., Maître, A., Ravaine, S., Chehimi, M.M., Mangeney, C., 2012. Inverse opals of molecularly imprinted hydrogels for the detection of bisphenol A and pH sensing. Langmuir 28, 1005–1012.
Guo, C., Zhou, C., Sai, N., Ning, B., Liu, M., Chen, H., et al., 2012. Detection of bisphenol A using an opal photonic crystal sensor. Sensors Actuators B 166, 17–23.
Haacke, G., Panzer, H.P., Magliocco, L.G., Asher, S.A., 1993. Narrow band radiation filter films. US Patent 5266238 A.
Hadziioannou, G., Skoulios, A., 1982. Molecular weight dependence of lamellar structure in styrene isoprene two-and three-block copolymers. Macromolecules 15, 258–262.
Haslam, R.H., 2003. Lead poisoning. Paediatr. Child Health 8, 509.
Hazell, A.S., Butterworth, R.F., 1999. Hepatic encephalopathy: an update of pathophysiologic mechanisms. Exp. Biol. Med. 222, 99–112.
He, J.-A., Valluzzi, R., Yang, K., Dolukhanyan, T., Sung, C., Kumar, J., et al., 1999. Electrostatic multilayer deposition of a gold–dendrimer nanocomposite. Chem. Mater. 11, 3268–3274.
Heskins, M., Guillet, J.E., 1968. J. Macromol. Sci. Chem. 2, 1441–1455.
Hinterholzinger, F.M., Ranft, A., Feckl, J.M., Ruhle, B., Bein, T., Lotsch, B.V., 2012. One-dimensional metal-organic framework photonic crystals used as platforms for vapor sorption. J. Mater. Chem. 22, 10356–10362.
Hisamitsu, I., Kataoka, K., Okano, T., Sakurai, Y., 1997. Glucose-responsive gel from phenylborate polymer and poly (vinyl alcohol): prompt response at physiological pH through the interaction of borate with amino group in the gel. Pharm. Res. 14, 289–293.
Holtz, J.H., Asher, S.A., 1997. Polymerized colloidal crystal hydrogel films as intelligent chemical sensing materials. Nature 389, 829–832.
Holtz, J.H., Holtz, J.S., Munro, C.H., Asher, S.A., 1998. Intelligent polymerized crystalline colloidal arrays: novel chemical sensor materials. Anal. Chem. 70, 780–791.
Hong, J., Lowack, K., Schmitt, J., Decher, G., 1993. Layer-by-layer deposited multilayer assemblies of polyelectrolytes and proteins: from ultrathin films to protein arrays. In: Laggner, P., Glatter, O. (Eds.), Trends in Colloid and Interface Science VII. Springer, pp. 98–102.
Hong, W., Li, H., Hu, X., Zhao, B., Zhang, F., Zhang, D., 2012. Independent multifunctional detection by wettability controlled inverse opal hydrogels. Chem. Commun. (Camb. U. K.) 48, 4609–4611.
Hong, W., Chen, Y., Feng, X., Yan, Y., Hu, X., Zhao, B., et al., 2013. Full-color CO_2 gas sensing by an inverse opal photonic hydrogel. Chem. Commun. (Camb. U. K.) 49, 8229–8231.
Hooke, R., 1665. Micrographia. J. Martyn and J. Allestry, London.
Horgan, A.M., Marshall, A.J., Kew, S.J., Dean, K.E.S., Creasey, C.D., Kabilan, S., 2006. Crosslinking of phenylboronic acid receptors as a means of glucose selective holographic detection. Biosens. Bioelectron. 21, 1838–1845.
Huang, H., Serpe, M.J., 2015. Poly (N-isopropylacrylamide) microgel-based etalons for determining the concentration of ethanol in gasoline. J. Appl. Polym. Sci. 132.
Hurtado, J.L., Lowe, C.R., 2014. Ammonia-sensitive photonic structures fabricated in nafion membranes by laser ablation. ACS Appl. Mater. Interfaces 6, 8903–8908.
Imran, A.B., Seki, T., Takeoka, Y., 2010. Recent advances in hydrogels in terms of fast stimuli responsiveness and superior mechanical performance. Polym. J. 42, 839–851.
Ingersoll, D., Kulesza, P.J., Faulkner, L.R., 1994. Polyoxometallate-based layered composite films on electrodes preparation through alternate immersions in modification solutions. J. Electrochem. Soc. 141, 140–147.
Islam, M.R., Serpe, M.J., 2014. A novel label-free colorimetric assay for DNA concentration in solution. Anal. Chim. Acta 843, 83–88.
Jiang, C., Ko, H., Tsukruk, V.V., 2005. Strain-sensitive Raman modes of carbon nanotubes in deflecting freely suspended nanomembranes. Adv. Mater. 17, 2127–2131.
Jiang, H., Markowski, J., Sabarinathan, J., 2009. Near-infrared optical response of thin film pH-sensitive hydrogel coated on a gold nanocrescent array. Opt. Express 17, 21802–21807.
Jiang, H., Zhu, Y., Chen, C., Shen, J., Bao, H., Peng, L., et al., 2012. Photonic crystal pH and metal cation sensors based on poly (vinyl alcohol) hydrogel. New J. Chem. 36, 1051–1056.
Jin, L., Zhao, Y., Liu, X., Wang, Y., Ye, B., Xie, Z., et al., 2012. Dual signal glucose reporter based on inverse opal conducting hydrogel films. Soft Matter 8, 4911–4917.
Joannopoulos, J.D., Johnson, S.G., Winn, J.N., Meade, R.D., 2011. Photonic Crystals: Molding the Flow of Light. 2 ed. Princeton University Press, United States.
Kabilan, S., Blyth, J., Lee, M.C., Marshall, A.J., Hussain, A., Yang, X.P., et al., 2004. Glucose-sensitive holographic sensors. J. Mol. Recognit. 17, 162–166.
Kabilan, S., Marshall, A.J., Sartain, F.K., Lee, M.C., Hussain, A., Yang, X.P., et al., 2005. Holographic glucose sensors. Biosens. Bioelectron. 20, 1602–1610.
Kado, S., Otani, H., Nakahara, Y., Kimura, K., 2013. Highly selective recognition of acetate and bicarbonate by thiourea-functionalised inverse opal hydrogel in aqueous solution. Chem. Commun. (Camb. U. K.) 49, 886–888.
Kalorama Information, 2014. The Market and Potential for Molecular Point of Care Diagnostics.
Kang, Y., Walish, J.J., Gorishnyy, T., Thomas, E.L., 2007. Broad-wavelength-range chemically tunable block-copolymer photonic gels. Nat. Mater. 6, 957–960.
Keller, S.W., Kim, H.-N., Mallouk, T.E., 1994. Layer-by-layer assembly of intercalation compounds and heterostructures on surfaces: toward molecular" beaker" epitaxy. J. Am. Chem. Soc. 116, 8817–8818.
Kim, J., Serpe, M.J., Lyon, L.A., 2004. Hydrogel microparticles as dynamically tunable microlenses. J. Am. Chem. Soc. 126, 9512–9513.
Kim, J., Nayak, S., Lyon, L.A., 2005a. Bioresponsive hydrogel microlenses. J. Am. Chem. Soc. 127, 9588–9592.
Kim, J., Serpe, M.J., Lyon, L.A., 2005b. Photoswitchable microlens arrays. Angew. Chem. Int. Ed. 44, 1333–1336.
Kim, J., Singh, N., Lyon, L.A., 2006. Label-free biosensing with hydrogel microlenses. Angew. Chem. Int. Ed. 45, 1446–1449.
Kim, J., Singh, N., Lyon, L.A., 2007a. Displacement-induced switching rates of bioresponsive hydrogel microlenses. Chem. Mater. 19, 2527–2532.
Kim, J., Singh, N., Lyon, L.A., 2007b. Influence of ancillary binding and nonspecific adsorption on bioresponsive hydrogel microlenses. Biomacromolecules 8, 1157–1161.
Kim, H.-C., Park, S.-M., Hinsberg, W.D., 2010. Block copolymer based nanostructures: materials, processes, and applications to electronics. Chem. Rev. 110, 146–177.
Kim, O.-H., Cho, Y.-H., Kang, S.H., Park, H.-Y., Kim, M., Lim, J.W., et al., 2013. Ordered macroporous platinum electrode and enhanced mass transfer in fuel cells using inverse opal structure. Nat. Commun. 4.
Kim, S.-H., Park, J.-G., Choi, T.M., Manoharan, V.N., Weitz, D.A., 2014. Osmotic-pressure-controlled concentration of colloidal particles in thin-shelled capsules. Nat. Commun. 5.
Kimble, K.W., Walker, J.P., Finegold, D.N., Asher, S.A., 2006. Progress toward the development of a point-of-care photonic crystal ammonia sensor. Anal. Bioanal. Chem. 385, 678–685.
Kleinfeld, E.R., Ferguson, G.S., 1994. Stepwise formation of multilayered nanostructural films from macromolecular precursors. Science 265, 370–373.

Klinger, D., Robb, M.J., Spruell, J.M., Lynd, N.A., Hawker, C.J., Connal, L.A., 2013. Supramolecular guests in solvent driven block copolymer assembly: from internally structured nanoparticles to micelles. Polym. Chem. 4, 5038–5042.

Kloxin, A.M., Kasko, A.M., Salinas, C.N., Anseth, K.S., 2009. Photodegradable hydrogels for dynamic tuning of physical and chemical properties. Science 324, 59–63.

Komatsu, H., Miyachi, M., Fujii, E., Citterio, D., Yamada, K., Sato, Y., et al., 2006. SPR sensor signal amplification based on dye-doped polymer particles. Sci. Technol. Adv. Mater. 7, 150–155.

Kong, W., Zhang, X., Gao, M.L., Zhou, H., Li, W., Shen, J.C., 1994. A new kind of immobilized enzyme multilayer based on cationic and anionic interaction. Macromol. Rapid Commun. 15, 405–409.

Kong, X.-T., Butt, H., Yetisen, A.K., Kangwanwatana, C., Montelongo, Y., Deng, S., et al., 2014. Enhanced reflection from inverse tapered nanocone arrays. Appl. Phys. Lett. 105, 053108.

Kong, X.-T., Khan, A.A., Kidambi, P.R., Deng, S., Yetisen, A.K., Dlubak, B., et al., 2015. Graphene-based ultrathin flat lenses. ACS Photon. 2, 200–207.

Kotov, N.A., 1999. Layer-by-layer self-assembly: the contribution of hydrophobic interactions. Nanostruct. Mater. 12, 789–796.

Kotov, N.A., Dekany, I., Fendler, J.H., 1995. Layer-by-layer self-assembly of polyelectrolyte-semiconductor nanoparticle composite films. J. Phys. Chem. 99, 13065–13069.

Kraiskii, A.V., Postnikov, V.A., Sultanov, T.T., Khamidulin, A.V., 2010. Holographic sensors for diagnostics of solution components. IEEE J. Quantum Electron. 40, 178–182.

Kratz, A., 2004. Laboratory reference values. N. Engl. J. Med. 351, 1548–1563.

Ku, K.H., Shin, J.M., Kim, M.P., Lee, C.-H., Seo, M.-K., Yi, G.-R., et al., 2014. Size-controlled nanoparticle-guided assembly of block copolymers for convex lens-shaped particles. J. Am. Chem. Soc. 136, 9982–9989.

Kuriu, Y., Kawamura, A., Uragami, T., Miyata, T., 2014. Formation of thin molecularly imprinted hydrogel layers with lectin recognition sites on SPR sensor chips by atom transfer radical polymerization. Chem. Lett. 43, 825–827.

Lavine, B.K., Oxenford, L., Kim, M., Kaval, N., Benjamin, M., Seitz, W., 2012. Novel turbidimetric method to study polymer swelling. Microchem. J. 103, 97–104.

Lee, K., Asher, S.A., 2000. Photonic crystal chemical sensors: pH and ionic strength. J. Am. Chem. Soc. 122, 9534–9537.

Lee, Y.J., Braun, P.V., 2003. Tunable inverse opal hydrogel pH sensors. Adv. Mater. 15, 563–566.

Lee, W., Pruzinsky, S.A., Braun, P.V., 2002. Multi-photon polymerization of waveguide structures within three-dimensional photonic crystals. Adv. Mater. 14, 271–274.

Lee, M.C., Kabilan, S., Hussain, A., Yang, X., Blyth, J., Lowe, C.R., 2004a. Glucose-sensitive holographic sensors for monitoring bacterial growth. Anal. Chem. 76, 5748–5755.

Lee, Y.-J., Pruzinsky, S.A., Braun, P.V., 2004b. Glucose-sensitive inverse opal hydrogels: analysis of optical diffraction response. Langmuir 20, 3096–3106.

Leite, E., Babeva, T., Ng, E.P., Toal, V., Mintova, S., Naydenova, I., 2010a. Optical properties of photopolymer layers doped with aluminophosphate nanocrystals. J. Phys. Chem. C 114, 16767–16775.

Leite, E., Naydenova, I., Mintova, S., Leclercq, L., Toal, V., 2010b. Photopolymerizable nanocomposites for holographic recording and sensor application. Appl. Opt. 49, 3652–3660.

Leith, E.N., Upatnieks, J., 1962. Reconstructed wavefronts and communication theory. J. Opt. Soc. Am. 52, 1123–1128.

Lelong, A., Hégaret, H., Soudant, P., Bates, S.S., 2012. Pseudo-nitzschia (Bacillariophyceae) species, domoic acid and amnesic shellfish poisoning: revisiting previous paradigms. Phycologia 51, 168–216.

Lendlein, A., Jiang, H., Jünger, O., Langer, R., 2005. Light-induced shape-memory polymers. Nature 434, 879–882.

Li, C., Lotsch, B.V., 2012. Stimuli-responsive 2D polyelectrolyte photonic crystals for optically encoded pH sensing. Chem. Commun. (Camb. U. K.) 48, 6169–6171.

Li, X., Peng, L., Cui, J., Li, W., Lin, C., Xu, D., et al., 2012. Reactive photonic film for label-free and selective sensing of cyanide. Small 8, 612–618.

Li, S., Yang, M., Zhou, W., Johnston, T.G., Wang, R., Zhu, J., 2015a. Dextran hydrogel coated surface plasmon resonance imaging (SPRi) sensor for sensitive and label-free detection of small molecule drugs. Appl. Surf. Sci 355, 570–576.

Li, X., Gao, Y., Serpe, M.J., 2015b. Reductant-responsive poly (N-isopropylacrylamide) microgels and microgel-based optical materials. Can. J. Chem. 93, 1–5.

Lim, H.S., Lee, J.-H., Walish, J.J., Thomas, E.L., 2012. Dynamic swelling of tunable full-color block copolymer photonic gels *via* counterion exchange. ACS Nano 6, 8933–8939.

Lin, F.-Y., Yu, L.-P., 2012. Thiourea functionalized hydrogel photonic crystal sensor for Cd^{2+} detection. Anal. Methods 4, 2838–2845.

Lippmann, G., 1894. Sur la Theorie de la Photographie des Couleurs Simples et Composees par la Methode Interferentielle. J. Phys. 3, 97–107.

Liu, S., Volkmer, D., Kurth, D.G., 2003. Functional polyoxometalate thin films *via* electrostatic layer-by-layer self-assembly. J. Clust. Sci. 14, 405–419.

Liu, C., Gao, G., Zhang, Y., Wang, L., Wang, J., Song, Y., 2012. The naked-eye detection of NH_3–HCl by polyaniline-infiltrated TiO_2 inverse opal photonic crystals. Macromol. Rapid Commun. 33, 380–385.

Lockwood, A.H., 2004. Blood ammonia levels and hepatic encephalopathy. Metab. Brain Dis. 19, 345–349.

Loh, X.J., Scherman, O.A., 2012. Polymeric and Self Assembled Hydrogels: From Fundamental Understanding to Applications. Royal Society of Chemistry, Cambridge, UK.

Loiseaux, B., Huignard, J.P., Dubois, J.C., Eranian, A., 1984. Process for producing diffracting phase structures. US Patent 06428162.

Lojou, É., Bianco, P., 2004. Buildup of polyelectrolyte–protein multilayer assemblies on gold electrodes. Role of the hydrophobic effect. Langmuir 20, 748–755.

Lotierzo, M., Henry, O.Y.F., Piletsky, S., Tothill, I., Cullen, D., Kania, M., et al., 2004. Surface plasmon resonance sensor for domoic acid based on grafted imprinted polymer. Biosens. Bioelectron. 20, 145–152.

Lotsch, B.V., Knobbe, C.B., Ozin, G.A., 2009. A step towards optically encoded silver release in 1D photonic crystals. Small 5, 1498–1503.

Lowe CR, Millington RB, Blyth J, Mayes AG. Hologram used as a sensor, WO Patent Application 1995026499 A1. 1995.

Lvov, Y., Decher, G., Sukhorukov, G., 1993. Assembly of thin films by means of successive deposition of alternate layers of DNA and poly (allylamine). Macromolecules 26, 5396–5399.

Lvov, Y., Ariga, K., Kunitake, T., 1994. Layer-by-layer assembly of alternate protein/polyion ultrathin films. Chem. Lett. 2323–2326.

Lvov, Y., Ariga, K., Ichinose, I., Kunitake, T., 1995. Assembly of multicomponent protein films by means of electrostatic layer-by-layer adsorption. J. Am. Chem. Soc. 117, 6117–6123.

Lvov, Y., Onda, M., Ariga, K., Kunitake, T., 1998. Ultrathin films of charged polysaccharides assembled alternately with linear polyions. J. Biomater. Sci. Polym. Ed. 9, 345–355.

Lynd, N.A., Meuler, A.J., Hillmyer, M.A., 2008. Polydispersity and block copolymer self-assembly. Prog. Polym. Sci. 33, 875–893.

Lyon, L.A., Debord, J.D., Debord, S.B., Jones, C.D., McGrath, J.G., Serpe, M.J., 2004. Microgel colloidal crystals. J. Phys. Chem. B 108, 19099–19108.

Ma, C., Jiang, Y., Yang, X., Wang, C., Li, H., Dong, F., et al., 2013. Centrifugation-induced water-tunable photonic colloidal crystals with narrow diffraction bandwidth and highly sensitive detection of SCN–. ACS Appl. Mater. Interfaces 5, 1990–1996.

MacConaghy, K.I., Chadly, D.M., Stoykovich, M.P., Kaar, J.L., 2015. Optically diffracting hydrogels for screening kinase activity in vitro and in cell lysate: impact of material and solution properties. Anal. Chem. 87, 3467–3475.

Mack, N.H., Wackerly, J.W., Malyarchuk, V., Rogers, J.A., Moore, J.S., Nuzzo, R.G., 2007. Optical transduction of chemical forces. Nano Lett. 7, 733–737.

Maddox, R.L., 1871. An experiment with gelatino-bromide. Br. J. Photogr. 18, 422–423.

Maiman, T.H., 1960. Stimulated optical radiation in ruby. Nature 187, 493–494.

Mamedov, A.A., Kotov, N.A., Prato, M., Guldi, D.M., Wicksted, J.P., Hirsch, A., 2002. Molecular design of strong single-wall carbon nanotube/polyelectrolyte multilayer composites. Nat. Mater. 1, 190–194.

Manikas, A., Aliberti, A., Causa, F., Battista, E., Netti, P., 2014. Thermoresponsive PNIPAAm hydrogel scaffolds with encapsulated AuNPs show high analyte-trapping ability and tailored plasmonic properties for high sensing efficiency. J. Mater. Chem. B 3, 53–58.

Mansfield, E., O'Leary, T.J., Gutman, S.I., 2005. Food and drug administration regulation of in vitro diagnostic devices. J. Mol. Diagn. 7, 2–7.

Markets&Markets, 2013. In Vitro Diagnostic (IVD) Market [Instruments, Reagents & Data Management Systems] [Technique (Immunoassay, Clinical Chemistry, Molecular Diagnostics, Haematology) & Applications (Diabetes, Infectious Diseases, Cancer & Cardiology)] Systems, End Users] — Forecast To 2017.

Marshall, A.J., Blyth, J., Davidson, C.A., Lowe, C.R., 2003. pH-sensitive holographic sensors. Anal. Chem. 75, 4423–4431.

Marshall, A.J., Young, D.S., Blyth, J., Kabilan, S., Lowe, C.R., 2004a. Metabolite-sensitive holographic biosensors. Anal. Chem. 76, 1518–1523.

Marshall, A.J., Young, D.S., Kabilan, S., Hussain, A., Blyth, J., Lowe, C.R., 2004b. Holographic sensors for the determination of ionic strength. Anal. Chim. Acta 527, 13–20.

Martinez, A.W., Phillips, S.T., Whitesides, G.M., 2008. Three-dimensional microfluidic devices fabricated in layered paper and tape. Proc. Natl. Acad. Sci. U. S. A. 105, 19606–19611.

Martinez-Hurtado, J.L., Davidson, C.A., Blyth, J., Lowe, C.R., 2010. Holographic detection of hydrocarbon gases and other volatile organic compounds. Langmuir 26, 15694–15699.

Martinez-Hurtado, J.L., Davidson, C.A.B., Lowe, C.R., 2011. Monitoring organic volatiles and flammable gases with a holographic sensor. In: Vo-Dinh, T., Lieberman, R.A., Gauglitz, G. (Eds.), Proc. SPIE Orlando, Florida 80240Y1-80240Y7.

Martinez-Hurtado, J.L., Akram, M.S., Yetisen, A.K., 2013. Iridescence in meat caused by surface gratings. Foods 2, 499–506.

Massé, P., Reculusa, S., Clays, K., Ravaine, S., 2006. Tailoring planar defect in three-dimensional colloidal crystals. Chem. Phys. Lett. 422, 251–255.

Matsen, M.W., Bates, F., 1996. Origins of complex self-assembly in block copolymers. Macromolecules 29, 7641–7644.

Mayer, K.M., Hafner, J.H., 2011. Localized surface plasmon resonance sensors. Chem. Rev. 111, 3828–3857.

Mayes, A.G., Blyth, J., Kyröläinen-Reay, M., Millington, R.B., Lowe, C.R., 1999. A holographic alcohol sensor. Anal. Chem. 71, 3390–3396.

Mayes, A.G., Blyth, J., Millington, R.B., Lowe, C.R., 2002. Metal ion-sensitive holographic sensors. Anal. Chem. 74, 3649–3657.

Mesch, M., Zhang, C., Braun, P.V., Giessen, H., 2015. Functionalized hydrogel on plasmonic nanoantennas for noninvasive glucose sensing. ACS Photon. 2, 475–480.

Mikulchyk, T., Martin, S., Naydenova, I., 2013. Humidity and temperature effect on properties of transmission gratings recorded in PVA/AA-based photopolymer layers. J. Opt. 15, 105301.

Mikulchyk, T., Martin, S., Naydenova, I., 2014. Investigation of the sensitivity to humidity of an acrylamide-based photopolymer containing N-phenylglycine as a photoinitiator. Opt. Mater. 37, 810–815.

Millington, R.B., Mayes, A.G., Blyth, J., Lowe, C.R., 1996. A hologram biosensor for proteases. Sensors Actuators B 33, 55–59.

Mishra, S.K., Gupta, B.D., 2013. Surface plasmon resonance based fiber optic pH sensor utilizing Ag/ITO/Al/hydrogel layers. Analyst 138, 2640–2646.

Mishra, S.K., Gupta, B.D., 2014. Surface plasmon resonance based fiber optic sensor for the detection of CrO_4^{2-} using Ag/ITO/hydrogel layers. Anal. Methods 6, 5191–5197.

Miyata, T., 2010. Preparation of smart soft materials using molecular complexes. Polym. J. 42, 277–289.

Morokoshi, S., Ohhori, K., Mizukami, K., Kitano, H., 2004. Sensing capabilities of colloidal gold modified with a self-assembled monolayer of a glucose-carrying polymer chain on a glass substrate†. Langmuir 20, 8897–8902.

Müller, M., 2001. Orientation of α-helical poly (L-lysine) in consecutively adsorbed polyelectrolyte multilayers on texturized silicon substrates. Biomacromolecules 2, 262–269.
Nakayama, D., Takeoka, Y., Watanabe, M., Kataoka, K., 2003. Simple and precise preparation of a porous gel for a colorimetric glucose sensor by a templating technique. Angew. Chem. 115, 4329–4332.
Naydenova, I., Jallapuram, R., Toal, V., Martin, S., 2008. A visual indication of environmental humidity using a color changing hologram recorded in a self-developing photopolymer. Appl. Phys. Lett. 92, 031109.
Naydenova, I., Jallapuram, R., Toal, V., Martin, S., 2009. Characterisation of the humidity and temperature responses of a reflection hologram recorded in acrylamide-based photopolymer. Sensors Actuators B 139, 35–38.
Naydenova, I., Jallapuram, R., Martin, S., Toal, V., 2011. Holographic humidity sensors. In: Okada, C.T. (Ed.), Humidity Sensors: Types, Nanomaterials and Environmental Monitoring. Nova Science Publishers, Hauppauge, pp. 117–142.
Newton, I., 1704. Opticks: Or, A Treatise of the Reflections, Refractions, Inflections and Colours of Light. Sam. Smith & Benj. Walford, London.
Nogueira, G.M., Banerjee, D., Cohen, R.E., Rubner, M.F., 2011. Spray-layer-by-layer assembly can more rapidly produce optical-quality multistack heterostructures. Langmuir 27, 7860–7867.
Nuopponen, M., Tenhu, H., 2007. Gold nanoparticles protected with pH and temperature-sensitive diblock copolymers. Langmuir 23, 5352–5357.
Ock, K., Jang, G., Roh, Y., Kim, S., Kim, J., Koh, K., 2001. Optical detection of Cu^{2+} ion using a SQ-dye containing polymeric thin-film on Au surface. Microchem. J. 70, 301–305.
Oh, J.-W., Chung, W.-J., Heo, K., Jin, H.-E., Lee, B.Y., Wang, E., et al., 2014. Biomimetic virus-based colourimetric sensors. Nat. Commun. 5.
Okumura, A., Sato, Y., Kyo, M., Kawaguchi, H., 2005. Point mutation detection with the sandwich method employing hydrogel nanospheres by the surface plasmon resonance imaging technique. Anal. Biochem. 339, 328–337.
Ouyang, L., Zhu, L., Jiang, J., Xie, W., Tang, H., 2015. Three-dimensional plasmonic hydrogel architecture: facile synthesis and its macroscale effective space. RSC Adv. 5, 2231–2238.
Palacios-Lidón, E., Galisteo-López, J.F., Juárez, B.H., López, C., 2004. Engineered planar defects embedded in opals. Adv. Mater. 16, 341–345.
Palmer, J.R., Wise, L.A., Hatch, E.E., Troisi, R., Titus-Ernstoff, L., Strohsnitter, W., et al., 2006. Prenatal diethylstilbestrol exposure and risk of breast cancer. Cancer Epidemiol. Biomark. Prev. 15, 1509–1514.
Pan, Z., Ma, J., Yan, J., Zhou, M., Gao, J., 2012. Response of inverse-opal hydrogels to alcohols. J. Mater. Chem. 22, 2018–2025.
Park, R., 2014. IVD Market Continues to Be Steady and Solid, Medical Design Technology Magazine.
Parmar, A., 2013. Global In Vitro Diagnostics Market to Grow To $69.1 billion by 2017. Medical Device and Diagnostic Industry Magazine.
Pike, J., Godbert, S., Johnson, S., 2013. Comparison of volunteers' experience of using, and accuracy of reading, different types of home pregnancy test formats. Expert Opin. Med. Diagn. 7, 435–441.
Pozas, R., Mihi, A., Ocaña, M., Míguez, H., 2006. Building nanocrystalline planar defects within self-assembled photonic crystals by spin-coating. Adv. Mater. 18, 1183–1187.
Price, C.P., Kricka, L.J., 2007. Improving healthcare accessibility through point-of-care technologies. Clin. Chem. 53, 1665–1675.
Pruzinsky, S.A., Braun, P.V., 2005. Fabrication and characterization of two-photon polymerized features in colloidal crystals. Adv. Funct. Mater. 15, 1995–2004.
Radic, Z., Pickering, N.A., Vellom, D.C., Camp, S., Taylor, P., 1993. Three distinct domains in the cholinesterase molecule confer selectivity for acetyl-and butyrylcholinesterase inhibitors. Biochemistry 32, 12074–12084.
Reese, C.E., Asher, S.A., 2003. Photonic crystal optrode sensor for detection of Pb^{2+} in high ionic strength environments. Anal. Chem. 75, 3915–3918.
Reese, C.E., Guerrero, C.D., Weissman, J.M., Lee, K., Asher, S.A., 2000. Synthesis of highly charged, monodisperse polystyrene colloidal particles for the fabrication of photonic crystals. J. Colloid Interface Sci. 232, 76–80.
Richert, L., Lavalle, P., Vautier, D., Senger, B., Stoltz, J.-F., Schaaf, P., et al., 2002. Cell interactions with polyelectrolyte multilayer films. Biomacromolecules 3, 1170–1178.
Roche, 2014. Annual Report. F. Hoffmann-La Roche AG.
Rochon, P.L., Lévesque, L., 2006. Standing wave surface plasmon mediated forward and backward scattering. Opt. Express 14, 13050–13055.
Rodríguez-Fernández, J., Fedoruk, M., Hrelescu, C., Lutich, A.A., Feldmann, J., 2011. Triggering the volume phase transition of core–shell Au nanorod–microgel nanocomposites with light. Nanotechnology 22, 245708.
Rooney, M.T.V., Seitz, W.R., 1999. An optically sensitive membrane for pH based on swellable polymer microspheres in a hydrogel. Anal. Commun. 36, 267–270.
Rosen, S., 2014. The Worldwide Market for In Vitro Diagnostic (IVD) Tests. 9th ed. Kalomara Information.
Rundquist, P.A., Photinos, P., Jagannathan, S., Asher, S.A., 1989. Dynamical Bragg diffraction from crystalline colloidal arrays. J. Chem. Phys. 91, 4932–4941.
Sai, N., Ning, B., Huang, G., Wu, Y., Zhou, Z., Peng, Y., et al., 2013. An imprinted crystalline colloidal array chemical-sensing material for detection of trace diethylstilbestrol. Analyst 138, 2720–2728.
Saito, H., Takeoka, Y., Watanabe, M., 2003. Simple and precision design of porous gel as a visible indicator for ionic species and concentration. Chem. Commun. (Camb. U. K.) 2126–2127.
Sartain, F.K., Yang, X.P., Lowe, C.R., 2006. Holographic lactate sensor. Anal. Chem. 78, 5664–5670.
Sartain, F.K., Yang, X.P., Lowe, C.R., 2008. Complexation of L-lactate with boronic acids: a solution and holographic analysis. Chem. Eur. J. 14, 4060–4067.
Schild, H., 1992. Poly (N-isopropylacrylamide): experiment, theory and application. Prog. Polym. Sci. 17, 163–249.
Schönhoff, M., 2003. Self-assembled polyelectrolyte multilayers. Curr. Opin. Colloid Interface Sci. 8, 86–95.
Serpe, M.J., Kim, J., Lyon, L.A., 2004. Colloidal hydrogel microlenses. Adv. Mater. 16, 184–187.
Shakhsher, Z., Seitz, W.R., Legg, K.D., 1994. Single fiber-optic pH sensor based on changes in reflection accompanying polymer swelling. Anal. Chem. 66, 1731–1735.
Sharma, A.C., Jana, T., Kesavamoorthy, R., Shi, L., Virji, M.A., Finegold, D.N., et al., 2004. A general photonic crystal sensing motif: creatinine in bodily fluids. J. Am. Chem. Soc. 126, 2971–2977.
Shields, D., Sale, A., 2014. Global In Vitro Diagnostics (IVD) Market (Technique, Product, Usability, Application, End User, and Geography) — Size, Share, Global Trends, Company Profiles, Demand, Insights, Analysis, Research, Report, Opportunities, Segmentation and Forecast, 2013–2020. Allied Market Research.
Shimamoto, C., Hirata, I., Katsu, K., 1999. Breath and blood ammonia in liver cirrhosis. Hepato-Gastroenterology 47, 443–445.
Shimazaki, Y., Mitsuishi, M., Ito, S., Yamamoto, M., 1997. Preparation of the layer-by-layer deposited ultrathin film based on the charge-transfer interaction. Langmuir 13, 1385–1387.
Siemens, 2014. Annual Report.
Singh, S., Gupta, B.D., 2012. Fabrication and characterization of a highly sensitive surface plasmon resonance based fiber optic pH sensor utilizing high index layer and smart hydrogel. Sensors Actuators B 173, 268–273.
Specht, E.H., Neuman, A., Hills, N., Neher, H.T., 1956. Preparation of Acrylamides. US Patent 2773063 A.
Spooncer, R.C., Al-Ramadhan, F.A.S., Jones, B.E., 1992. A humidity sensor using a wavelength-dependent holographic filter with fibre optic links. Int. J. Optoelectron. 7, 449–452.
Springsteen, G., Wang, B., 2002. A detailed examination of boronic acid–diol complexation. Tetrahedron 58, 5291–5300.
St John, A., Price, C.P., 2014. Existing and emerging technologies for point-of-care testing. Clin. Biochem. Rev. 35, 155.
Stuart, M.A.C., Huck, W.T., Genzer, J., Müller, M., Ober, C., Stamm, M., et al., 2010. Emerging applications of stimuli-responsive polymer materials. Nat. Mater. 9, 101–113.
Sun, J., Wu, T., Sun, Y., Wang, Z., Zhang, X., Shen, J., et al., 1998. Fabrication of a covalently attached multilayer *via* photolysis of layer-by-layer self-assembled films containing diazo-resins. Chem. Commun. (Camb. U. K.) 1853–1854.
Taguchi, Y., Takano, E., Takeuchi, T., 2012. SPR sensing of bisphenol a using molecularly imprinted nanoparticles immobilized on slab optical waveguide with consecutive parallel Au and Ag deposition bands coexistent with bisphenol a-immobilized Au nanoparticles. Langmuir 28, 7083–7088.
Takeoka, Y., Watanabe, M., 2003. Template synthesis and optical properties of chameleonic poly (N-isopropylacrylamide) gels using closest-packed self-assembled colloidal silica crystals. Adv. Mater. 15, 199–201.
Takeoka, Y., Watanabe, M., Yoshida, R., 2003. Self-sustaining peristaltic motion on the surface of a porous gel. J. Am. Chem. Soc. 125, 13320–13321.
Tan, E.V., Lowe, C.R., 2009. Holographic enzyme inhibition assays for drug discovery. Anal. Chem. 81, 7579–7589.
Tétreault, N., Mihi, A., Míguez, H., Rodríguez, I., Ozin, G.A., Meseguer, F., et al., 2004. Dielectric planar defects in colloidal photonic crystal films. Adv. Mater. 16, 346–349.
Tétreault, N., von Freymann, G., Deubel, M., Hermatschweiler, M., Pérez-Willard, F., John, S., et al., 2006. New route to three-dimensional photonic bandgap materials: silicon double inversion of polymer templates. Adv. Mater. 18, 457–460.
Tian, T., Li, X., Cui, J., Li, J., Lan, Y., Wang, C., et al., 2014. Highly sensitive assay for acetylcholinesterase activity and inhibition based on a specifically reactive photonic nanostructure. ACS Appl. Mater. Interfaces 6, 15456–15465.
Tikhonov, A., Kornienko, N., Zhang, J.-T., Wang, L., Asher, S.A., 2012. Reflectivity enhanced two-dimensional dielectric particle array monolayer diffraction. J. Nanophotonics 6, 063509-1–063509-9.
Tokareva, I., Minko, S., Fendler, J.H., Hutter, E., 2004. Nanosensors based on responsive polymer brushes and gold nanoparticle enhanced transmission surface Plasmon resonance spectroscopy. J. Am. Chem. Soc. 126, 15950–15951.
Tokareva, I., Tokarev, I., Minko, S., Hutter, E., Fendler, J.H., 2006. Ultrathin molecularly imprinted polymer sensors employing enhanced transmission surface plasmon resonance spectroscopy. Chem. Commun. (Camb. U. K.) 3343–3345.
Tonyushkina, K., Nichols, J.H., 2009. Glucose meters: a review of technical challenges to obtaining accurate results. J. Diabetes Sci. Technol. 3, 971–980.
Trope, I., Lopez-Villegas, D., Cecil, K.M., Lenkinski, R.E., 2001. Exposure to lead appears to selectively alter metabolism of cortical gray matter. Pediatrics 107, 1437–1443.
Tsangarides, C.P., Yetisen, A.K., Vasconcellos, F.D., Montelongo, Y., Qasim, M.M., Wilkinson, T.D., et al., 2014. Computational modelling and characterisation of nanoparticle-based tuneable photonic crystal sensors. RSC Adv. 4, 10454–10461.
Ueno, K., Matsubara, K., Watanabe, M., Takeoka, Y., 2007. An electro- and thermochromic hydrogel as a full-color indicator. Adv. Mater. 19, 2807–2812.
Um, S.H., Lee, J.B., Park, N., Kwon, S.Y., Umbach, C.C., Luo, D., 2006. Enzyme-catalysed assembly of DNA hydrogel. Nat. Mater. 5, 797–801.
Urbas, A., Fink, Y., Thomas, E.L., 1999. One-dimensionally periodic dielectric reflectors from self-assembled block copolymer–homopolymer blends. Macromolecules 32, 4748–4750.
Urbas, A.M., Maldovan, M., DeRege, P., Thomas, E.L., 2002. Bicontinuous cubic block copolymer photonic crystals. Adv. Mater. 14, 1850–1853.
Vasconcellos, F.C., Yetisen, A.K., Montelongo, Y., Butt, H., Grigore, A., Davidson, C.A., et al., 2014. Printable surface holograms *via* laser ablation. ACS Photon. 1, 489–495.
Vekris, E., Kitaev, V., von Freymann, G., Perovic, D.D., Aitchison, J.S., Ozin, G.A., 2005. Buried linear extrinsic defects in colloidal photonic crystals. Adv. Mater. 17, 1269–1272.
Verma, R., Gupta, B.D., 2013. Fiber optic SPR sensor for the detection of 3-pyridinecarboxamide (vitamin B3) using molecularly imprinted hydrogel. Sensors Actuators B 177, 279–285.

Vignolini, S., Rudall, P.J., Rowland, A.V., Reed, A., Moyroud, E., Faden, R.B., et al., 2012. Pointillist structural color in *Pollia* fruit. Proc. Natl. Acad. Sci. U. S. A. 109, 15712–15715.
Volpatti, L.R., Yetisen, A.K., 2014. Commercialization of microfluidic devices. Trends Biotechnol. 32, 347–350.
von Freymann, G., Kitaev, V., Lotsch, B.V., Ozin, G.A., 2013. Bottom-up assembly of photonic crystals. Chem. Soc. Rev. 42, 2528–2554.
Vukusic, P., Sambles, J.R., 2003. Photonic structures in biology. Nature 424, 852–855.
Walker, J.P., Asher, S.A., 2005. Acetylcholinesterase-based organophosphate nerve agent sensing photonic crystal. Anal. Chem. 77, 1596–1600.
Wang, Z., Zhang, J., Li, J., Xie, J., Li, Y., Liang, S., et al., 2011. Colorful detection of organic solvents based on responsive organic/inorganic hybrid one-dimensional photonic crystals. J. Mater. Chem. 21, 1264–1270.
Wang, P., Zhang, L., Xia, Y., Tong, L., Xu, X., Ying, Y., 2012. Polymer nanofibers embedded with aligned gold nanorods: a new platform for plasmonic studies and optical sensing. Nano Lett. 12, 3145–3150.
Wei Chang, W., Chi Chiu, C., Yi Fan, Z., Kam, C.L., 2012. Miniature single-mode fiber refractive index interferometer sensor based on high order cladding mode and core-offset. IEEE Photon. Technol. Lett. 24, 359–361.
Wichterle, O., Lim, D., 1960. Hydrophilic Gels for Biological use. Nature 185, 117–118.
Wong, W.C., Chan, C.C., Hu, P., Chan, J.R., Low, Y.T., Dong, X., et al., 2014. Miniature pH optical fiber sensor based on waist-enlarged bitaper and mode excitation. Sensors Actuators B 191, 579–585.
Worsley, G.J., Tourniaire, G.A., Medlock, K.E., Sartain, F.K., Harmer, H.E., Thatcher, M., et al., 2007. Continuous blood glucose monitoring with a thin-film optical sensor. Clin. Chem. 53, 1820–1826.
Worsley, G.J., Tourniaire, G.A., Medlock, K.E., Sartain, F.K., Harmer, H.E., Thatcher, M., et al., 2008. Measurement of glucose in blood with a phenylboronic acid optical sensor. J. Diabetes Sci. Technol. 2, 213–220.
Wulff, G., 1995. Molecular imprinting in cross-linked materials with the aid of molecular templates—a way towards artificial antibodies. Angew. Chem. Int. Ed. Engl. 34, 1812–1832.
Xia, Y., Gates, B., Yin, Y., Lu, Y., 2000. Monodispersed colloidal spheres: old materials with new applications. Adv. Mater. 12, 693–713.
Xiao, X.-C., Chu, L.-Y., Chen, W.-M., Wang, S., Xie, R., 2004. Preparation of submicrometer-sized monodispersed thermoresponsive core–shell hydrogel microspheres. Langmuir 20, 5247–5253.
Xing, J.-F., Zheng, M.-L., Duan, X.-M., 2015. Two-photon polymerization microfabrication of hydrogels: an advanced 3D printing technology for tissue engineering and drug delivery. Chem. Soc. Rev. 44, 5031–5039.
Xue, F., Meng, Z., Qi, F., Xue, M., Wang, F., Chen, W., et al., 2014a. Two-dimensional inverse opal hydrogel for pH sensing. Analyst 139, 6192–6196.
Xue, F., Meng, Z., Wang, Y., Huang, S., Wang, Q., Lu, W., et al., 2014b. A molecularly imprinted colloidal array as a colorimetric sensor for label-free detection of p-nitrophenol. Anal. Methods 6, 831–837.
Yang, X., Lee, M.C., Sartain, F., Pan, X., Lowe, C.R., 2006. Designed boronate ligands for glucose-selective holographic sensors. Chemistry 12, 8491–8497.
Yang, X.P., Pan, X.H., Blyth, J., Lowe, C.R., 2008. Towards the real-time monitoring of glucose in tear fluid: holographic glucose sensors with reduced interference from lactate and pH. Biosens. Bioelectron. 23, 899–905.
Ye, B.-F., Zhao, Y.-J., Li, T.-T., Xie, Z.-Y., Gu, Z.-Z., 2011. Aptamer-based suspension array indexed by structural color and shape. J. Mater. Chem. 21, 18659–18664.
Yee, C.K., Jordan, R., Ulman, A., White, H., King, A., Rafailovich, M., et al., 1999. Novel one-phase synthesis of thiol-functionalized gold, palladium, and iridium nanoparticles using superhydride. Langmuir 15, 3486–3491.
Yeo, S.J., Tu, F., Kim, S.-H., Yi, G.-R., Yoo, P.J., Lee, D., 2015. Angle-and strain-independent coloured free-standing films incorporating non-spherical colloidal photonic crystals. Soft Matter 11, 1582–1588.
Yetisen, A.K., 2015a. Fundamentals of Holographic Sensing. Springer International Publishing, Cham, Switzerland, pp. 27–51.
Yetisen, A.K., 2015b. Holographic Glucose Sensors. Holographic Sensors. Cham. Springer International Publishing, Switzerland, pp. 101–134.
Yetisen, A.K., 2015c. Holographic metal ion sensors. Holographic Sensors. Springer International Publishing, Cham, Switzerland, pp. 85–99.
Yetisen, A.K., 2015d. Holographic pH sensors. Holographic Sensors. Springer International Publishing, Cham, Switzerland, pp. 53–83.
Yetisen, A.K., 2015e. Mobile medical applications. Holographic Sensors. Springer International Publishing, Cham, Switzerland, pp. 135–148.
Yetisen, A.K., 2015f. Point-of-care diagnostics. Holographic Sensors. Springer International Publishing, Cham, Switzerland, pp. 1–25.
Yetisen, A.K., 2015g. The prospects for holographic sensors. Holographic Sensors. Springer International Publishing, Cham, Switzerland, pp. 149–162.
Yetisen, A.K., Volpatti, L.R., 2014. Patent protection and licensing in microfluidics. Lab Chip 14, 2217–2225.
Yetisen, A.K., Akram, M.S., Lowe, C.R., 2013. Paper-based microfluidic point-of-care diagnostic devices. Lab Chip 13, 2210–2251.
Yetisen, A.K., Butt, H., Vasconcellos, F.D., Montelongo, Y., Davidson, C.A.B., Blyth, J., et al., 2014a. Light-directed writing of chemically tunable narrow-band holographic sensors. Adv. Opt. Mater. 2, 250–254.
Yetisen, A.K., Martinez-Hurtado, J.L., da Cruz, V.F., Simsekler, M.C.E., Akram, M.S., Lowe, C.R., 2014b. The regulation of mobile medical applications. Lab Chip 14, 833–840.
Yetisen, A.K., Martinez-Hurtado, J.L., Garcia-Melendrez, A., da Cruz, V.F., Lowe, C.R., 2014c. A smartphone algorithm with inter-phone repeatability for the analysis of colorimetric tests. Sensors Actuators B 196, 156–160.
Yetisen, A.K., Montelongo, Y., da Cruz, V.F., Martinez-Hurtado, J.L., Neupane, S., Butt, H., et al., 2014d. Reusable, robust, and accurate laser-generated photonic nanosensor. Nano Lett. 14, 3587–3593.
Yetisen, A.K., Montelongo, Y., Farandos, N.M., Naydenova, I., Lowe, C.R., Yun, S.H., 2014e. Mechanism of multiple grating formation in high-energy recording of holographic sensors. Appl. Phys. Lett. 105, 261106.
Yetisen, A.K., Naydenova, I., da Cruz, V.F., Blyth, J., Lowe, C.R., 2014f. Holographic sensors: three-dimensional analyte-sensitive nanostructures and their applications. Chem. Rev. 114, 10654–10696.
Yetisen, A.K., Qasim, M.M., Nosheen, S., Wilkinson, T.D., Lowe, C.R., 2014g. Pulsed laser writing of holographic nanosensors. J. Mater. Chem. C 2, 3569.
Yetisen, A.K., Montelongo, Y., Qasim, M.M., Butt, H., Wilkinson, T.D., Monteiro, M.J., et al., 2015a. Photonic nanosensor for colorimetric detection of metal ions. Anal. Chem. 87, 5101–5108.
Yetisen, A.K., Volpatti, L.R., Coskun, A.F., Cho, S., Kamrani, E., Butt, H., et al., 2015b. Entrepreneurship. Lab Chip 15, 3638–3660.
Yoo, P.J., Nam, K.T., Qi, J., Lee, S.-K., Park, J., Belcher, A.M., et al., 2006. Spontaneous assembly of viruses on multilayered polymer surfaces. Nat. Mater. 5, 234–240.
Yoon, J., Lee, W., Thomas, E.L., 2008. Thermochromic block copolymer photonic gel. Macromolecules 41, 4582–4584.
Young, T., 1804. Experimental demonstration of the general law of the interference of light. Phil. Trans. R. Soc. London 94, 1–16.
Yuan, Y., Li, Z., Liu, Y., Gao, J., Pan, Z., Liu, Y., 2012. Hydrogel photonic sensor for the detection of 3-pyridinecarboxamide. Chem. Eur. J. 18, 303–309.
Zaarour, M., Dong, B., Naydenova, I., Retoux, R., Mintova, S., 2014. Progress in zeolite synthesis promotes advanced applications. Microporous Mesoporous Mater. 189, 11–21.
Zeng, F., Wu, S., Sun, Z., Xi, H., Li, R., Hou, Z., 2002. Urea sensing materials *via* solidified crystalline colloidal arrays. Sensors Actuators B 81, 273–276.
Zeng, X., Du, Z., Ma, J., 2012. Colorimetric detection of ultratrace cholesterol by free standing inverse opal hydrogel films. Optical Sensors. Optical Society of America, Monterey, CA, p. STh1B. 5.
Zhai, L., Nolte, A.J., Cohen, R.E., Rubner, M.F., 2004. pH-gated porosity transitions of polyelectrolyte multilayers in confined geometries and their application as tunable Bragg reflectors. Macromolecules 37, 6113–6123.
Zhang, C., Losego, M.D., Braun, P.V., 2013a. Hydrogel-based glucose sensors: effects of phenylboronic acid chemical structure on response. Chem. Mater. 25, 3239–3250.
Zhang, J.-T., Chao, X., Liu, X., Asher, S.A., 2013b. Two-dimensional array Debye ring diffraction protein recognition sensing. Chem. Commun. (Camb. U. K.) 49, 6337–6339.
Zhang, M.-L., Jin, F., Zheng, M.-L., Duan, X.-M., 2014. Inverse opal hydrogel sensor for the detection of pH and mercury ions. RSC Adv. 4, 20567–20572.
Zhang, Q.M., Ahiabu, A., Gao, Y., Serpe, M.J., 2015. CO2-switchable poly (N-isopropylacrylamide) microgel-based etalons. J. Mater. Chem. C 3, 495–498.
Zhao, Y., Wostyn, K., de Schaetzen, G., Clays, K., Hellemans, L., Persoons, A., et al., 2003. The fabrication of photonic band gap materials with a two-dimensional defect. Appl. Phys. Lett. 82, 3764–3766.
Zhao, Y., Zhao, X., Gu, Z., 2010a. Photonic crystals in bioassays. Adv. Funct. Mater. 20, 2970–2988.
Zhao, Y., Zhao, X., Tang, B., Xu, W., Gu, Z., 2010b. Rapid and sensitive biomolecular screening with encoded macroporous hydrogel photonic beads. Langmuir 26, 6111–6114.
Zhao, Y., Zhao, X., Tang, B., Xu, W., Li, J., Hu, J., et al., 2010c. Quantum-dot-tagged bioresponsive hydrogel suspension array for multiplex label-free DNA detection. Adv. Funct. Mater. 20, 976–982.
Zhao, Y., Xie, Z., Gu, H., Zhu, C., Gu, Z., 2012. Bio-inspired variable structural color materials. Chem. Soc. Rev. 41, 3297–3317.
Zhao, Y., Shang, L., Cheng, Y., Gu, Z., 2014. Spherical colloidal photonic crystals. Acc. Chem. Res. 47, 3632–3642.
Zhao, Q., Yetisen, A.K., Anthony, C.J., Fowler, W.R., Yun, S.H., Butt, H., 2015a. Printable ink holograms. Appl. Phys. Lett. 107, 041115.
Zhao, Q., Yetisen, A.K., Sabouri, A., Yun, S.H., Butt, H., 2015b. Printable nanophotonic devices *via* holographic laser ablation. ACS Nano 9, 9062–9069.
Zhong, Q., Xu, H., Ding, H., Bai, L., Mu, Z., Xie, Z., et al., 2013. Preparation of conducting polymer inverse opals and its application as ammonia sensor. Colloids Surf. A 433, 59–63.